isvr Institute of Sound and Vibration Research

Sound Transmission Testing at Low Frequencies

T. Bravo and S.J. Elliott

ISVR Technical Memorandum 921

October 2003

University of Southampton

SCIENTIFIC PUBLICATIONS BY THE ISVR

Technical Reports are published to promote timely dissemination of research results by ISVR personnel. This medium permits more detailed presentation than is usually acceptable for scientific journals. Responsibility for both the content and any opinions expressed rests entirely with the author(s).

Technical Memoranda are produced to enable the early or preliminary release of information by ISVR personnel where such release is deemed to the appropriate. Information contained in these memoranda may be incomplete, or form part of a continuing programme; this should be borne in mind when using or quoting from these documents.

Contract Reports are produced to record the results of scientific work carried out for sponsors, under contract. The ISVR treats these reports as confidential to sponsors and does not make them available for general circulation. Individual sponsors may, however, authorize subsequent release of the material.

UNIVERSITY OF SOUTHAMPTON

INSTITUTE OF SOUND AND VIBRATION RESEARCH

SIGNAL PROCESSING & CONTROL GROUP

Sound Transmission Testing at Low Frequencies

by

T. Bravo and S. J. Elliott

ISVR Technical Memorandum No. 921

October 2003

Authorised for issue by
Prof S J Elliott
Group Chairman

Acknowledgements

This research has been supported through a European Marie Curie Fellowship, Contract N° HPMF-CT-2002-01618.

Contents

Tables

Figures

Abstract

This paper discusses the characterisation of low frequency sound transmission between two rooms via a flexible panel. A fully-coupled modal model is used to investigate the individual effect of the source room and the receiving room on the measured sound reduction index, and the results compared with the ideal case of having a free field on both sides of the panel. The effect of the source room on the measured sound reduction index at low frequencies can be reduced by using a number of suitable-driven loudspeakers close to the panel to simulate a diffuse incident field. However, the effect of the receiving room was found not to be reduced by calculating the transmitted acoustic power from a dense array of acoustic intensity measurements, instead of an array of microphones in the receiving room.

SOUND TRANSMISSION TESTING AT LOW FREQUENCIES

1. INTRODUCTION

Characterisation of the sound reduction index of panels is of prime importance in industries like automotive and aerospace. The fundamental theories for sound transmission through panels are derived under the condition that the sound field in both rooms is ideally diffuse (Nilsson, 1972; Fahy, 1985; Beranek and Vér, 1992). In practice, panels are often tested by subjecting them to acoustic excitation in finite sized reverberant chambers.

In such a test, an acoustic field is generated by several loudspeakers in the source room and the sound is transmitted into the receiving room via the panel under test. As the frequency of excitation increases, the modal density and modal overlap in the enclosures also increases. In a "random incident" sound field, the sound is incident on the separating partition from all angles with approximately equal probability (Beranek and Vér, 1992). The acoustic field can be assumed to be the diffuse field value when the modal density is sufficiently high. Below this region, the modal behaviour of the cavities is important and the diffuse approximation is no longer valid.

Large differences are observed at low frequencies between the predicted and measured transmission loss, and between the reduction indices for the same type of panel measured in different transmission suites. The fact that room dimensions can be of importance for the acoustic tests has been pointed out in several papers. Utley (1968) established that the situation was not satisfactory, especially when one wishes to compare low frequency results from several facilities, due to the properties of the reverberant chambers in which the measurements were made. In a paper by Quirt (1982) the transmission loss data from an extensive series of nominally equivalent laboratory measurements are presented, showing important differences due to properties of both the samples and the laboratories.

It is, thus, of particular interest to investigate the feasibility of experimentally reproducing a diffuse acoustic pressure field using an array of loudspeakers in the sound transmission suite (Elliott *et al.*, 2001; Maury *et al.*, 2002). The laboratory simulation of the diffuse field would allow the transmission loss measurements to be performed over the whole frequency range, without limitations at low frequencies where the cavities exhibit modal characteristics. Also, this accurate experimental description can be used as a prediction tool for the engineering design of sound barriers, based until now on classical analytical formulae and prediction methods that are currently limited, especially in the low frequency domain (Sgard *et al.*, 2000).

For the study of the configuration used to test the structures in a real situation, it is necessary to analyse the coupled structural-acoustic system composed by the source and the receiving room

separated by a wall and the partition between them. An acoustic field is produced in the source room by a set of loudspeakers that excites the panel and the receiving room. An analytical model can be used in the low frequency range in terms of infinite series of weighted normal modes for the subsystems. The acoustic field in the two rooms and the panel velocity are derived as functions of the source strengths.

The report is organised as follows: In Section 2 the theory of sound transmission in terms of the modal characteristic of the uncoupled subsystems is developed. The vibro-acoustic problem is studied using different coupling approximations and the results are illustrated with some numerical simulations, investigating the convergence of the solution and analysing the differences. Section 3 calculates the sound reduction index for three different situations: in the transmission loss suite, radiating to free field and mounted on an infinite baffle. The differences between the three characterisations are clearly seen when compared together. A signal processing formulation in presented in the next section for the reproduction of a diffuse acoustic pressure field using an array of loudspeakers, in terms of the spectral density matrix of the outputs on an array of sensors. The feasibility of the reproduction is analysed again in the three different configurations in terms of several error criteria. Finally, the conclusions are presented in the last section.

2. MODAL THEORY OF SOUND TRANSMISSION

Before studying the feasibility of reproducing low frequency sound transmission between a source room and a receiving room separated by a common panel, it is necessary to determine the response of the coupled vibro-acoustic system to exciting sources. A theoretical model of the acoustic pressure of a cavity due to the motion of the surrounding structure, and the acoustical loading of vibrating boundaries by a cavity has been formulated by Pope (1971), Dowell *et al.* (1977) and Fahy (1985). In these models, weak coupling is normally assumed, limiting the study to stiffened lightweight structures coupled to a contiguous lightly damped acoustic space.

Weak coupling allows the *in-vacuo* modal response of the structure and the response of a rigidly enclosed space to be used to determine the coupled system response. The two uncoupled modal models may then be coupled via modal coupling theory. The formulation of the response of the problem only depends on the modal properties of the subsystems involved and the nature of the excitation.

2.1 Modal characteristics of the uncoupled subsystems

The properties of the coupled problem can be obtained from its free solution, whose modal properties are fundamental to the system. In this section the main equations for the normal modes, characteristic frequencies and modal excitation terms are presented. First the acoustic pressure is derived in terms of the normal modes of a cavity surrounded by rigid walls, and the equations of motion of the structure are derived in terms of the *in-vacuo* structural normal modes. A time dependence of the form $e^{j\omega t}$ has been assumed in the analysis.

2.1.1 Cavity pressure field

An expression for the sound pressure at a point $\mathbf{r}$ in an enclosure of volume V can be expressed as a sum of modal terms of the form (Nelson and Elliott, 1992):

$$p(\mathbf{r},\omega) = \sum_{k=0}^{\infty} a_k^{(a)}(\omega)\psi_k(\mathbf{r}), \tag{2.1}$$

where $a_k^{(a)}(\omega)$ is the complex amplitude of the kth acoustic pressure mode defined by the mode shape function $\psi_k(\mathbf{r})$ and the natural frequency ω_k.

The modal amplitudes are given by

$$a_k^{(a)}(\omega) = A_k^{(a)}(\omega)\int_V S(\mathbf{r})\psi_k(\mathbf{r})\mathrm{d}V \ . \tag{2.2}$$

In this equation, $A_k^{(a)}(\omega)$ is the modal resonance term, expressed as:

$$A_k^{(a)}(\omega) = \frac{\rho_0 c_0^2 \omega}{M_k^{(a)}[2\omega B_k + \mathrm{j}(\omega^2 - \omega_k^2)]}\ , \tag{2.3}$$

where ρ_0 is the fluid density, c_0 the speed of sound in the fluid and B_k is the 3-dB (half power) bandwidth of the kth acoustic mode, which is assumed to have viscous damping. $M_k^{(a)}$ is the modal volume of the cavity mode, defined as the volume integration of the square mode shape through the cavity, that is:

$$M_k^{(a)} = \int_V \psi_k^2(\mathbf{r})\, \mathrm{d}V\ . \tag{2.4}$$

The term $S(\mathbf{r})$ in Eq. (2.2) is the distribution of acoustic source strength density (volume velocity per unit volume) at frequency ω in the room. Defining the generalised volume velocity as

$$q_k(\omega) = \int_V S(\mathbf{r})\psi_k(\mathbf{r})\mathrm{d}V\ , \tag{2.5}$$

the modal amplitude can be expressed in the form:

$$a_k^{(a)}(\omega) = A_k^{(a)}(\omega) q_k(\omega)\ . \tag{2.6}$$

This set of equations characterises the modal behaviour of the rigid–wall cavity.

2.1.2 Motion of the panel

An expression for the structural velocity at a point $\mathbf{r}_p$ on the structure can be derived in terms of its normal modes, and expressed as (Fuller et al., 1996):

$$v(\mathbf{r}_p, \omega) = \sum_{s=1}^{\infty} a_s^{(p)}(\omega)\phi_s(\mathbf{r}_p), \tag{2.7}$$

where $a_s^{(p)}(\omega)$ is the complex amplitude of the s th structural mode defined by the mode shape function $\phi_s(\mathbf{r}_p)$ and the natural frequency ω_s.

The modal amplitudes are given by:

$$a_s^{(p)}(\omega) = A_s^{(p)}(\omega) \int_{S_p} f(\mathbf{r}_p)\phi_s^{(p)}(\mathbf{r}_p)\mathrm{d}S\ , \tag{2.8}$$

where S_p denotes the surface area of the panel and $f(\mathbf{r}_p)$ is the force distribution per unit area. The modal resonance term is then

$$A_s^{(p)}(\omega) = \frac{\omega}{\mathrm{j}M_s^{(p)}[\omega^2 - (1+\mathrm{j}\eta)\omega_s^2)]}\ , \tag{2.9}$$

in which a hysteretic damping factor η has been assumed and $M_s^{(p)}$ is the modal mass, given by

$$M_s^{(p)} = \int_{S_p} m(\mathbf{r}_p)\phi_s^{(p)}(\mathbf{r}_p)\,\mathrm{d}S \ . \tag{2.10}$$

The constant $m(\mathbf{r}_p)$ is the surface density of the structure.

Defining the generalised force distribution as:

$$f_s(\omega) = \int_{S_p} f(\mathbf{r}_p)\phi_s^{(p)}(\mathbf{r}_p)\mathrm{d}S \ , \tag{2.11}$$

the amplitudes of the panel take the form:

$$a_s^{(p)}(\omega) = A_s^{(p)}(\omega)\, f_s(\omega) \, . \tag{2.12}$$

This set of equations characterises the modal behaviour of the *in-vacuo* panel.

2.2 Coupling between a cavity and a panel

The complete fluid-structural equations of motion can be obtained by coupling the previous expressions for the modal properties of the cavity and the structure. A schematic illustration of the problem is indicated in Figure 2.1. In this case, external forces and the acoustic pressure inside the enclosed cavity induce the motion of the flexible wall. This motion causes the fluid inside the cavity also to oscillate. The forces acting on the flexible wall are, thus, modified due to the coupling between the structure and the fluid, hence affecting the behaviour of the flexible wall and the acoustic behaviour of the enclosed cavity. This process is known as sound-structure interaction.

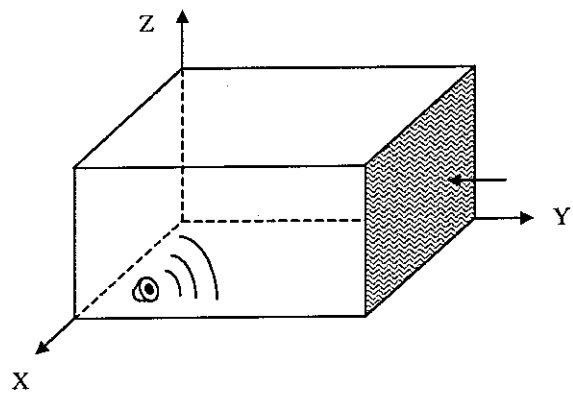

Figure 2.1. Physical arrangement of coupled system

The approach that will be followed here is presented by Dowell *et al.* (1977), and has been particularised to rectangular cavity systems by Pan and Bies (1990). Snyder and Hansen (1994) have applied the modal coupling theory to active noise and vibration control for weakly coupled structural

acoustic systems. The results have been generalised by Cazzolato (2000) to include the gyrostatic coupling terms.

The coupled modal equations of motion for the cavity in terms of the pressure field show a dependency on two different sources, the vibration of the panel due to pressure fluctuations and the acoustic sources inside the cavity. The corresponding modal amplitudes thus read:

$$a_a^{(a)} = \frac{\rho_0 c_0^2 \omega}{M_k[2B_s\omega + \mathrm{j}(\omega^2 - \omega_s^2)]}\left(-\sum_{s=1}^{\infty} a_s^{(p)} G_{ks} + q_k\right). \tag{2.13}$$

Similarly, the equations for the structure in terms of the normal velocity are due to the fluid pressure on the surface of the panel and the force applied to the panel, in the form:

$$a_s^{(p)} = \frac{\omega}{\mathrm{j}M_s^{(p)}[\omega^2 - (1+\mathrm{j}\eta)\omega_s^2)]}\left(\sum_{k=0}^{\infty} a_k^{(a)} G_{ks} + f_s\right), \tag{2.14}$$

where the term G_{ks} is the modal coupling coefficient between the kth acoustic mode and the sth structural mode. It is defined by:

$$G_{ks} = \int_{S_p} \psi_k \phi_s \, \mathrm{d}S \,. \tag{2.15}$$

This term governs the coupling between the panel and the cavity. If there is no spatial matching between one or more acoustic and structural modes, the uncoupled modes will be present in the system; if the coefficient is not zero, the coupled corresponding modes will differ from the original uncoupled ones.

2.3 Coupling between two rectangular rooms via a panel

The general modal approach developed in the previous sections will be particularised now for two rooms coupled via a common panel. For structures that have a simple geometry, like rectangular chambers, it is possible to model the system using analytical descriptions for the mode shapes of the structure and the acoustic enclosures.

A schematic representation of the system under study can be seen in Figure 2.2. The two rooms, with dimensions $a_1 \times b_1 \times c_1$, and $a_2 \times b_2 \times c_2$, are connected via a panel of dimensions $b_p \times c_p$. We assume for the sake of generality that the two rooms are not necessarily the same size, nor share any common edge. The panel may also extend over only part of the common edge. The coordinate system used is shown in Figure 2.2, together with the common wall boundary lying in the $x = 0$ plane for both rooms.

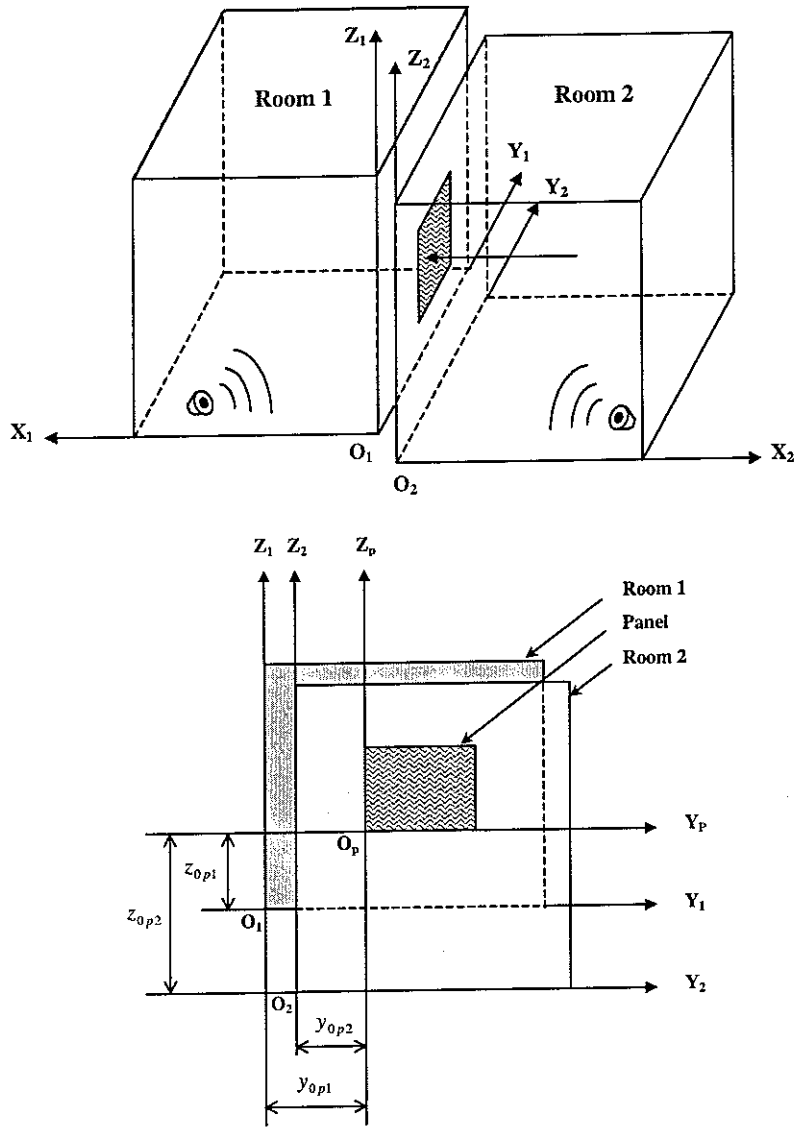

Figure 2.2. Sharing physical set-up

The complex pressure in the rectangular rooms at frequency ω is expanded as a modal series of the form:

$$p^{(1)}(x_1, y_1, z_1; \omega) = \sum_{l_1 m_1 n_1 = 0}^{\infty} a^{(1)}_{l_1 m_1 n_1}(\omega) \psi^{(1)}_{l_1 m_1 n_1}(x_1, y_1, z_1), \tag{2.16}$$

$$p^{(2)}(x_2, y_2, z_2; \omega) = \sum_{l_2 m_2 n_2 = 0}^{\infty} a^{(2)}_{l_2 m_2 n_2}(\omega) \psi^{(2)}_{l_2 m_2 n_2}(x_2, y_2, z_2), \tag{2.17}$$

where l, m and n are the modal integers of the mode shapes in the x, y and z directions respectively.

As the geometry of the problem is regular, there exists a well-known analytical description for the mode shapes and natural frequencies of the cavities and the panel, given as:

$$\psi_{l,m,n}(x,y,z)=\sqrt{\varepsilon_l\varepsilon_m\varepsilon_n}\cos\left(\frac{l\pi x}{a}\right)\cos\left(\frac{m\pi y}{b}\right)\cos\left(\frac{n\pi z}{c}\right), \tag{2.18}$$

$$\omega_{l,m,n}=\pi c_0\left[\left(\frac{l}{a}\right)^2+\left(\frac{m}{b}\right)^2+\left(\frac{n}{c}\right)^2\right]^{1/2}, \tag{2.19}$$

in which the constants ε_i are given by :

$$\varepsilon_i=\begin{cases}1 & \text{if } i=0\\ 2 & \text{if } i>0.\end{cases} \tag{2.20}$$

These constants are chosen so that the volume integral of the squared mode shape throughout the cavity is equal to its volume

$$V=\int_V \psi_i^2(\mathbf{r})\,\mathrm{d}V\ . \tag{2.21}$$

The modal resonance term then becomes:

$$A_{lmn}^{(a)}(\omega)=\frac{\rho_0 c_0^2\omega}{V[2\omega B_{lmn}+\mathrm{j}(\omega^2-\omega_{lmn}^2)]}\ . \tag{2.22}$$

A model of the acoustic damping has been calculated from the mode shapes and the average absorption coefficient of the walls, $\overline{\alpha}$, assumed independent of frequency, as follows (Nelson and Elliott, 1992):

$$B_{lmn}=\frac{c_0\overline{\alpha}}{8V}(\varepsilon_l s_x+\varepsilon_m s_y+\varepsilon_n s_z)\,. \tag{2.23}$$

The source of excitation has been modelled as a square piston situated at $x=x_s$, having uniform velocity distribution over its surface, S_s, and complex source strength q_s. The term $S(\mathbf{r})$ has the following expression

$$S(x,y,z)=\frac{q_s}{S_s}\delta(x-x_s)\,, \tag{2.24}$$

where $\delta(x)$ is the one-dimensional spatial Dirac delta function and S_s is the area of the piston source. The generalised volume velocity thus becomes:

$$q_{lmn}(\omega)=\int_V S(x,y,z)\psi_{lmn}(x,y,z)\,dV=\frac{q_s}{S_s}\int_{S_s}\psi_{lmn}(x_s,y,z)\,\mathrm{d}S\ . \tag{2.25}$$

Assuming that the panel is simply supported, the structural mode shapes and the natural frequencies, may be written as:

$$\phi_{qr}(y_p, z_p)=2\sin\left(\frac{q\pi y_p}{b_p}\right)\sin\left(\frac{r\pi z_p}{c_p}\right), \tag{2.26}$$

$$\omega_{qr}=\pi^2\sqrt{\frac{D}{m}}\left[\left(\frac{q}{b_p}\right)^2+\left(\frac{r}{c_p}\right)^2\right]. \tag{2.27}$$

In this equations, q and r are modal integers, b_p and c_p are the panel dimensions, D is the flexural stiffness of the panel and m its surface density. The factor of 2 is introduced so that the integral of the squared mode shape over the panel is equal to its surface, that is:

$$S_p m=\int_{S_p} m\phi_s^2(\mathbf{r}_p)\,\mathrm{d}S\ , \tag{2.28}$$

where S_p denotes the surface area of the panel $(b_p\times c_p)$.

Using the modal characteristics of the structural and acoustic subsystems, it is possible to define the coupling term between them. The modal equations of motion for room 1, for the panel and for room 2 are given by:

$$a^{(1)}_{l_1m_1n_1}=\frac{\rho_0c_0^2\omega}{V_1[2B_{l_1m_1n_1}\omega+\mathrm{j}(\omega^2-\omega^2_{l_1m_1n_1})]}\left(-\sum_{qr=1}^{\infty}a^{(p)}_{qr}G^{(1)}_{l_1m_1n_1,qr}+q^{(1)}_{l_1m_1n_1}\right) \tag{2.29}$$

$$a^{(p)}_{qr}=\frac{\omega}{\mathrm{j}mS_p[\omega^2-(1+\mathrm{j}\eta)\omega^2_{qr})]}\left(\sum_{l_1m_1n_1=0}^{\infty}a^{(1)}_{l_1m_1n_1}G^{(1)}_{l_1m_1n_1,qr}-\sum_{l_2m_2n_2=0}^{\infty}a^{(2)}_{l_2m_2n_2}G^{(2)}_{l_2m_2n_2,qr}+f_{qr}\right) \tag{2.30}$$

$$a^{(2)}_{l_2m_2n_2}=\frac{\rho_0c_0^2\omega}{V_2[2B_{l_2m_2n_2}\omega+\mathrm{j}(\omega^2-\omega^2_{l_2m_2n_2})]}\left(\sum_{qr=1}^{\infty}a^{(p)}_{qr}G^{(2)}_{l_2m_2n_2,qr}+q^{(2)}_{l_2m_2n_2}\right), \tag{2.31}$$

where the terms $G^{(1)}$ and $G^{(2)}$ are the modal coupling coefficient between the cavities and the panel, which have the expression:

$$\begin{aligned}G^{(1)}_{l_1m_1n_1qr}=&\frac{2}{\pi^2}S_p\sqrt{\varepsilon_{l_1}\varepsilon_{m_1}\varepsilon_{n_1}}\frac{q}{\left\{q^2-[m_1(b_p/b_1)]^2\right\}}\frac{r}{\left\{r^2-[n_1(c_p/c_1)]^2\right\}}\\&\times\left[\cos\pi\left(m_1\frac{b_p+y_{0p1}}{b_1}-q\right)-\cos\pi\left(m_1\frac{y_{0p1}}{b_1}\right)\right]\\&\times\left[\cos\pi\left(n_1\frac{c_p+z_{0p1}}{c_1}-r\right)-\cos\pi\left(n_1\frac{z_{0p1}}{c_1}\right)\right]\end{aligned} \tag{2.32}$$

$$G^{(2)}_{l_2m_2n_2,qr} = \frac{2}{\pi^2} S_p \sqrt{\varepsilon_{l_2}\varepsilon_{m_2}\varepsilon_{n_2}} \frac{q}{\left\{q^2 - [m_2(b_p/b_2)]^2\right\}} \frac{r}{\left\{r^2 - [n_2(c_p/c_2)]^2\right\}}$$
$$\times\left[\cos\pi\left(m_2\frac{b_p + y_{0p2}}{b_2} - q\right) - \cos\pi\left(m_2\frac{y_{0p2}}{b_2}\right)\right] \tag{2.33}$$
$$\times\left[\cos\pi\left(n_2\frac{c_p + z_{0p2}}{c_2} - r\right) - \cos\pi\left(n_2\frac{z_{0p2}}{c_2}\right)\right],$$

where (y_{0p1}, z_{0p1}) and (y_{0p2}, z_{0p2}) specify the position of the lower right-hand corner of the panel with respect to cavity 1 and cavity 2, respectively (see Figure 2.2).

Eqs. (2.29-2.31) constitute a coupled system that can be solved applying different approaches. In the following sections several approximations will be used to calculate the response.

2.3.1 Weakly coupled system

The problem of sound transmission from one room to another through a panel is addressed in this section. An acoustic field is generated by several loudspeakers in room 1, the source room, and is transmitted into room 2, the receiving room via the panel. This system has been analysed previously by Jo and Elliott (1991) to investigate the possibility of using active control for the low-frequency sound transmitted from one room to the other. In this case, weak coupling is assumed, with the following assumptions made for the sake of simplicity:

- All the walls, except the panel, do not vibrate.
- The sound is transmitted from the source into the receiving room via the panel, with no flanking transmission paths.
- The radiation from the panel back into the source room is negligible in comparison with that from the primary source.
- The response of the panel is not affected by the acoustic field in the receiving room.

Under these assumptions, the system of Eqs. (2.29-2.31) simplifies into:

$$a^{(1)}_{l_1m_1n_1} = \frac{\rho_0 c_0^2 \omega}{V_1[2B_{l_1m_1n_1}\omega + \mathrm{j}(\omega^2 - \omega^2_{l_1m_1n_1})]} q^{(1)}_{l_1m_1n_1} \tag{2.34}$$

$$a^{(p)}_{qr} = \frac{\omega}{\mathrm{j}mS_p[\omega^2 - (1+\mathrm{j}\eta)\omega^2_{qr})]} \sum_{l_1m_1n_1=0}^{\infty} a^{(1)}_{l_1m_1n_1} G^{(1)}_{l_1m_1n_1,qr} \tag{2.35}$$

$$a^{(2)}_{l_2m_2n_2} = \frac{\rho_0 c_0^2 \omega}{V_2[2B_{l_2m_2n_2}\omega + \mathrm{j}(\omega^2 - \omega^2_{l_2m_2n_2})]} \sum_{qr=1}^{\infty} a^{(p)}_{qr} G^{(2)}_{l_2m_2n_2,qr}\,. \tag{2.36}$$

The modal amplitudes of the pressure field in room 1 due to the presence of a primary source is expressed in Eq. (2.34), and can be substituted in Eq. (2.35) to obtain the structural response as follows:

$$a_{qr}^{(p)} = \frac{\omega}{\mathrm{j}ms_p[\omega^2 - (1+\mathrm{j}\eta)\omega_{qr}^2)]} \sum_{l_1 m_1 n_1 = 0}^{\infty} A_{l_1 m_1 n_1}^{(1)} G_{l_1 m_1 n_1, qr}^{(1)} q_{l_1 m_1 n_1}^{(1)} \tag{2.37}$$

The field in the receiving room after substituting Eq. (2.37) into Eq. (2.36) is, in this case:

$$a_{l_2 m_2 n_2}^{(2)} = A_{l_2 m_2 n_2}^{(2)} \left(\sum_{qr=1}^{\infty} \sum_{l_1 m_1 n_1 = 0}^{\infty} A_{qr}^{(p)} A_{l_1 m_1 n_1}^{(1)} G_{l_1 m_1 n_1, qr}^{(1)} G_{l_2 m_2 n_2, qr}^{(2)} q_{l_1 m_1 n_1}^{(1)} \right) \tag{2.38}$$

In practice, the sum cannot be extended to an infinite number of modes. If we use $N^{(1)}$ modes for the source room, $N^{(p)}$ modes for the panel and $N^{(2)}$ modes for the receiving room, the equations of the modal pressure and velocity amplitudes can be rewritten in matrix form in terms of the generalised volume velocity vector as

$$\mathbf{a}^{(1)} = \mathbf{A}^{(1)} \mathbf{Q}^{(1)} \tag{2.39}$$

$$\mathbf{a}^{(p)} = \mathbf{a}^{(1)} \mathbf{B}_p = \mathbf{A}^{(1)} \mathbf{Q}^{(1)} \mathbf{B}_p \tag{2.40}$$

$$\mathbf{a}^{(2)} = \mathbf{B}_2 \mathbf{a}^{(p)} = \mathbf{B}_2 \mathbf{B}_p \mathbf{A}^{(1)} \mathbf{Q}^{(1)}, \tag{2.41}$$

where $\mathbf{a}^{(1)}$, $\mathbf{a}^{(p)}$ and $\mathbf{a}^{(2)}$ are the pressure and velocity amplitude vectors of dimensions $(N^{(1)} \times 1)$, $(N^{(p)} \times 1)$ and $(N^{(2)} \times 1)$ respectively. $\mathbf{A}^{(1)}$ is a diagonal matrix of dimensions $(N^{(1)} \times N^{(1)})$, whose diagonal elements are given by Eq. (2.22), $\mathbf{Q}^{(1)}$ is the $(N^{(1)} \times 1)$ vector of generalised volume velocity source, whose elements are given by Eq. (2.25), $\mathbf{B}_p$ is a matrix of dimensions $(N^{(1)} \times N^{(p)})$, whose elements are given by Eq. (2.35) and $\mathbf{B}_2$ is a matrix of dimensions $(N^{(2)} \times N^{(p)})$, whose elements are given by Eq. (2.36).

2.3.2 Fully coupled system

In this section it is assumed that the pressure field in the source room is influenced by the panel motion, and this is coupled with the pressure field in both the source and the receiving rooms. We still suppose that there is no flanking transmission path in the system.

The system of Eqs. (2.29-2.31) becomes, after neglecting the force terms and the volume velocity term in room 2:

$$a_{l_1m_1n_1}^{(1)} = \frac{\rho_0 c_0^2 \omega}{V_1[2B_{l_1m_1n_1}\omega + \mathrm{j}(\omega^2 - \omega_{l_1m_1n_1}^2)]}\left(-\sum_{qr=1}^{\infty} a_{qr}^{(p)} G_{l_1m_1n_1,qr}^{(1)} + q_{l_1m_1n_1}^{(1)} \right) \tag{2.42}$$

$$a_{qr}^{(p)} = \frac{\omega}{\mathrm{j}mS_p[\omega^2 - (1+\mathrm{j}\eta)\omega_{qr}^2)]}\left(\sum_{l_1m_1n_1=0}^{\infty} a_{l_1m_1n_1}^{(1)} G_{l_1m_1n_1,qr}^{(1)} - \sum_{l_2m_2n_2=0}^{\infty} a_{l_2m_2n_2}^{(2)} G_{l_2m_2n_2,qr}^{(2)} \right) \tag{2.43}$$

$$a_{l_2m_2n_2}^{(2)} = \frac{\rho_0 c_0^2 \omega}{V_2[2B_{l_2m_2n_2}\omega + \mathrm{j}(\omega^2 - \omega_{l_2m_2n_2}^2)]}\left(\sum_{qr=1}^{\infty} a_{qr}^{(p)} G_{l_2m_2n_2,qr}^{(2)} \right). \tag{2.44}$$

Substituting now the modal panel amplitudes, Eq. (2.43), into Eqs. (2.42) and (2.44), we obtain

$$\begin{aligned} a_{l_1m_1n_1}^{(1)} &= \frac{\rho_0 c_0^2 \omega}{V_1[2B_{l_1m_1n_1}\omega + \mathrm{j}(\omega^2 - \omega_{l_1m_1n_1}^2)]} \\ &\times\left[-\sum_{qr=1}^{\infty} A_{qr}^{(p)} \left(\sum_{l_1'm_1'n_1'=0}^{\infty} a_{l_1'm_1'n_1'}^{(1)} G_{l_1'm_1'n_1',qr}^{(1)} - \sum_{l_2m_2n_2=0}^{\infty} a_{l_2m_2n_2}^{(2)} G_{l_2m_2n_2,qr}^{(2)} \right) G_{l_1m_1n_1,qr}^{(1)} + q_{l_1m_1n_1}^{(1)} \right] \end{aligned} \tag{2.45}$$

$$\begin{aligned} a_{l_2m_2n_2}^{(2)} &= \frac{\rho_0 c_0^2 \omega}{V_2[2B_{l_2m_2n_2}\omega + \mathrm{j}(\omega^2 - \omega_{l_2m_2n_2}^2)]} \\ &\times\left[\sum_{qr=1}^{\infty} A_{qr}^{(p)} \left(\sum_{l_1'm_1'n_1'=0}^{\infty} a_{l_1'm_1'n_1'}^{(1)} G_{l_1'm_1'n_1',qr}^{(1)} - \sum_{l_2'm_2'n_2'=0}^{\infty} a_{l_2'm_2'n_2'}^{(2)} G_{l_2'm_2'n_2',qr}^{(2)} \right) G_{l_2m_2n_2,qr}^{(2)} \right]. \end{aligned} \tag{2.46}$$

After rearrangement, it reads:

$$\begin{aligned} &\frac{V_1[2B_{l_1m_1n_1}\omega + \mathrm{j}(\omega^2 - \omega_{l_1m_1n_1}^2)]}{\rho_0 c_0^2 \omega} a_{l_1m_1n_1}^{(1)} + \sum_{qr=1}^{\infty} \sum_{l_1'm_1'n_1'=0}^{\infty} A_{qr}^{(p)} G_{l_1'm_1'n_1',qr}^{(1)} G_{l_1m_1n_1,qr}^{(1)} a_{l_1'm_1'n_1'}^{(1)} \\ &-\sum_{qr=1}^{\infty} \sum_{l_2m_2n_2=0}^{\infty} A_{qr}^{(p)} G_{l_2m_2n_2,qr}^{(2)} G_{l_1m_1n_1,qr}^{(1)} a_{l_2m_2n_2}^{(2)} = q_{l_1m_1n_1}^{(1)} \end{aligned} \tag{2.47}$$

$$\begin{aligned} &\frac{V_2[2B_{l_2m_2n_2}\omega + \mathrm{j}(\omega^2 - \omega_{l_2m_2n_2}^2)]}{\rho_0 c_0^2 \omega} a_{l_2m_2n_2}^{(2)} + \sum_{qr=1}^{\infty} \sum_{l_2'm_2'n_2'=0}^{\infty} A_{qr}^{(p)} G_{l_2'm_2'n_2',qr}^{(2)} G_{l_2m_2n_2,qr}^{(2)} a_{l_2'm_2'n_2'}^{(2)} \\ &-\sum_{qr=1}^{\infty} \sum_{l_1m_1n_1=0}^{\infty} A_{qr}^{(p)} G_{l_1m_1n_1,qr}^{(1)} G_{l_2m_2n_2,qr}^{(2)} a_{l_1m_1n_1}^{(1)} = 0. \end{aligned} \tag{2.48}$$

In a similar way, expressing these equations in matrix form, results in the following expressions:

$$\begin{aligned} \mathbf{Z}_1 \mathbf{a}^{(1)} + \mathbf{Z}_a^{(1)} \mathbf{a}^{(2)} &= \mathbf{Q}^{(1)} \\ \mathbf{Z}_a^{(2)} \mathbf{a}^{(1)} + \mathbf{Z}_2 \mathbf{a}^{(2)} &= \mathbf{0}, \end{aligned} \tag{2.49}$$

where $\mathbf{Z}_1$ is the $(N^{(1)} \times N^{(1)})$ matrix defined by

$$Z_{l_1m_1n_1,l_1'm_1'n_1'} = \begin{cases} \sum_{qr=1}^{\infty} A_{qr}^{(p)} G_{l_1'm_1'n_1',qr}^{(1)} G_{l_1m_1n_1,qr}^{(1)} & \text{if } l_1'm_1'n_1' \neq l_1m_1n_1 \\ \sum_{qr=1}^{\infty} A_{qr}^{(p)} G_{l_1m_1n_1,qr}^{(1)} G_{l_1m_1n_1,qr}^{(1)} + \dfrac{V_1[2B_{l_1m_1n_1}\omega + j(\omega^2 - \omega_{l_1m_1n_1}^2)]}{\rho_0 c_0^2 \omega} & \text{otherwise} \end{cases} \tag{2.50}$$

$\mathbf{Z}_2$ is the $(N^{(2)} \times N^{(2)})$ equivalent matrix for the second cavity, and $\mathbf{Z}_a^{(1)}$, with dimensions $(N^{(1)} \times N^{(2)})$ is defined as

$$Z_{a\, l_1m_1n_1,l_2m_2n_2} = -\sum_{qr=1}^{\infty} A_{qr}^{(p)} G_{l_2m_2n_2,qr}^{(2)} G_{l_1m_1n_1,qr}^{(1)} . \tag{2.51}$$

$\mathbf{Z}_a^{(2)}$ is the $(N^{(2)} \times N^{(1)})$ equivalent matrix for the second cavity.

2.4 Numerical simulations

The equations derived in the previous section for the pressure fields in the rooms and the velocity of the panel for the coupled system have been implemented in a Matlab program. The first system analysed is the same than the one by Jo and Elliott (1992), and was motivated by an experimental investigation in a sound transmission suite in the ISVR. The two reverberant rooms were coupled via a glass panel fixed in a square aperture, as indicated in Figure 2.2.

2.4.1 Glass partition

The physical constants used for the simulations are presented in Table 2.1, and were chosen to be similar to those measured in the physical set-up (Jo, 1990).

Table 2.1. Physical constants used for the numerical simulation

Subsystem	Material Property	Value
Air	*Density*	1.21 kg/m^3
	Speed of sound	343 m/s
Source room	*Dimensions*	2.07 x 2.52 x 2.51 m
	Absorption coefficient	0.11
Receiving room	*Dimensions*	2.38 x 2.53 x 2.62 m
	Absorption coefficient	0.08
Glass	*Dimensions*	0.69 x 0.69 m
	Thickness	0.006 m
	Mass per unit area	13.8 Kg m^{-2}
	Flexural stiffness	1184 Nm
	Hysteretic loss factor	0.9

The number of significantly excited acoustic modes in the two rooms, and the number of significantly excited panel modes assumed in the various summations was 127, 151 and 8 respectively, which included all modes with natural frequencies below 400 Hz. The first 20 natural frequencies of these acoustic and structural modes are listed in Table 2.2.

Table 2.2. Natural frequencies (Hz) of the first 20 modes

Mode	Source room	Receiving room	Panel
1	0	0	61.1207
2	68.0556	65.4580	152.8016
3	68.3267	67.7866	152.8016
4	82.8502	72.0588	244.4826
5	96.4370	94.2325	305.6033
6	107.2181	97.3510	305.6033
7	107.3904	98.9318	397.2843
8	127.1387	118.6265	397.2843
9	136.1111	130.9160	519.5256
10	136.6534	135.5731	519.5256
11	152.2983	144.1176	550.0859
12	152.6621	147.4246	611.2065
13	159.3436	149.4372	611.2065
14	159.8071	150.5484	764.0082
15	165.7005	153.5335	764.0082
16	173.3751	158.2866	794.5685
17	173.6948	159.2637	794.5685
18	179.1318	164.0930	886.2495
19	179.2350	166.9051	886.2495
20	191.7205	172.1908	977.9305

The response simulation of the system was calculated using a square piston source of dimensions 0.1 x 0.1 m, placed in a corner of the source room, at position (2.0, 0.117, 0.093) m. The acoustic impedances for the response points situated at positions (0.02, 1.1, 1.1) m for the source room and (0.02, 1.1, 1.2) m for the receiving room are shown in Figure 2.3(a) and (c) respectively. The panel volume/velocity volume transfer function for the position (0.3, 0.3) m is represented in Figure 2.3(b). Both approximations, weakly and totally coupled system are compared in the figure. As it can be observed, the transmission loss is relatively high for this particular case, and the assumptions made supposing that the source room is not affected by the panel and the sound field in the receiving room has a negligible reaction in the partition are a convenient idealisation that allows a simplified model of the problem.

In order to observe significant differences between the two approximations it would be necessary to consider a fluid with a higher density in contact with the panel, i.e. water, small volume cavities or the sound transmission between a whole wall rather than a partition. As these cases cannot occur in the ISVR experimental set-up, it will not be further investigated here. An example presented in Figure 2.4 is obtained using a glass panel with a thickness equal to 0.001 m and a hysteretic loss factor with a value of 0.005. As it can be seen, the assumptions for the weakly coupled system do not hold in this case, with differences between the weakly and fully cases up to 20 dB.

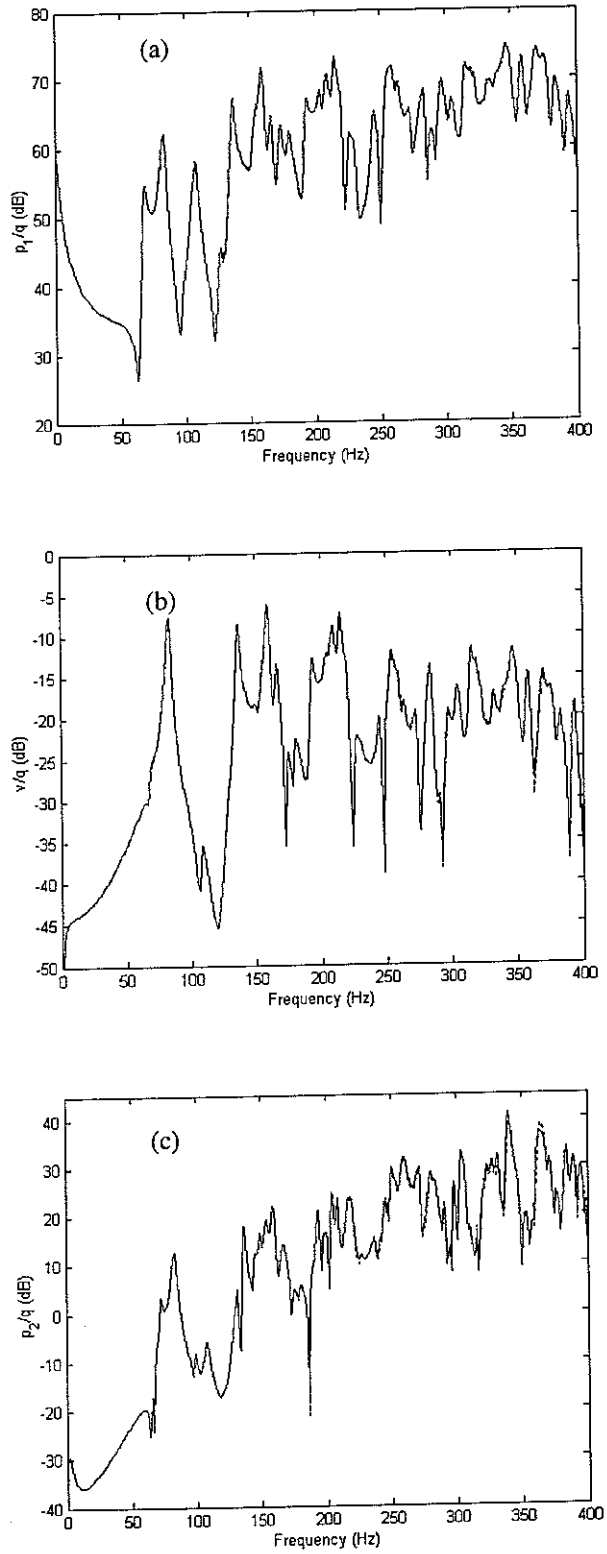

Figure 2.3. Acoustic impedance with thick heavily- damped panel in the source room (a) and in the receiving room (c), and panel velocity/volume velocity transfer function (b), calculated considering a partially coupled system (solid line) and a fully-coupled system (dashed line)

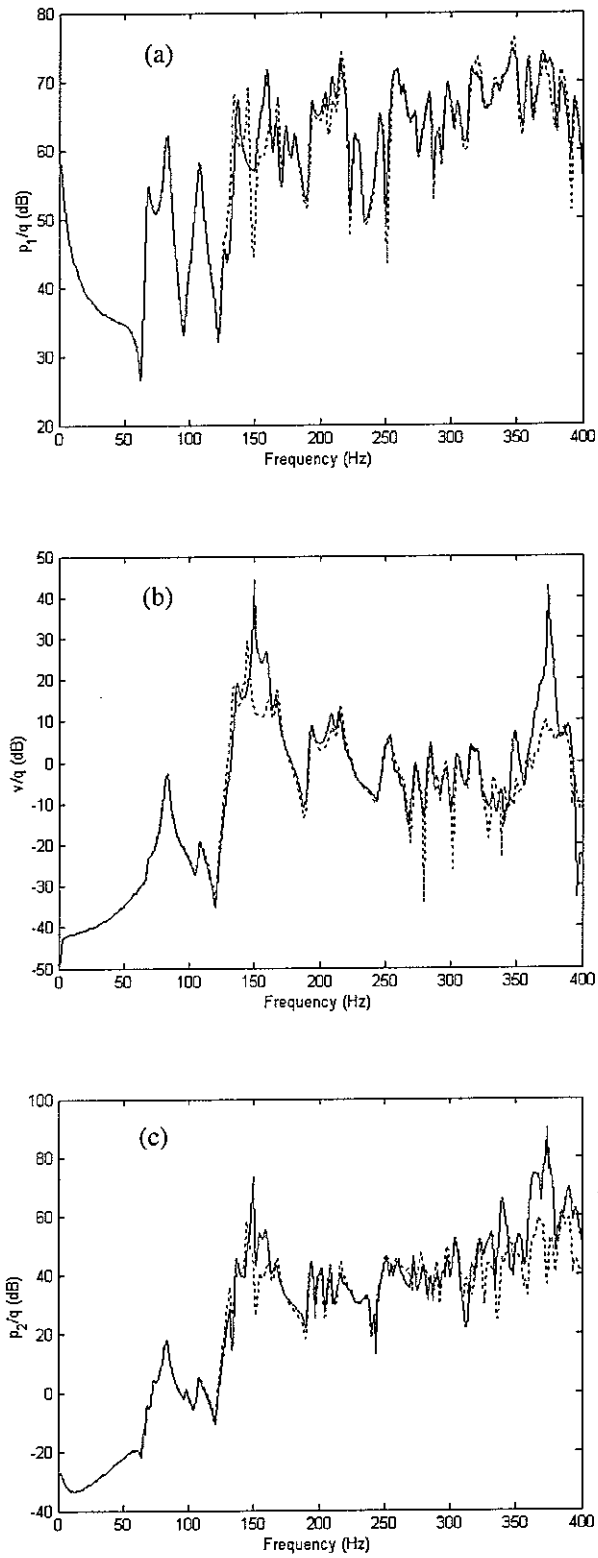

Figure 2.4. Acoustic impedance with thin lightly- damped panel in the source room (a) and in the receiving room (c), and panel velocity/volume velocity transfer function (b), calculated considering a partially coupled system (solid line) and a fully-coupled system (dashed line)

2.4.2 Aluminium partition

In the previous section, the differences between the weakly and fully coupled modal systems and the factors than can influence the results obtained with each method have been presented briefly. In this part several aspects of the transmission cavities via an aluminium partition will be analysed, in particular the convergence of the proposed modal model. The panel was assumed to have a thickness of 0.003 m, a Young's modulus of 70.3 GPa, a density of 2700 Kg/m^3 and a Poisson's ratio of 0.35.

Since the analysis of the coupled behaviour of the system uses the *in vacuo* structural modes and the rigid walled model for the cavities, the velocity predicted at the partition does not converge towards the exact value. The pressure field is accurate in the interior of the cavity but can differ substantially in the vicinity of the vibrating surface (Fahy, 1985; Jayachandran *et al.*, 1998), and the effect of modal truncation could be critical for the convergence of the method. In particular, the total number of normal modes required in the simulation programs, such that a trade-off can be found between the calculation time and the accuracy of the solution has been studied in detail, analysing the convergence of the fully coupled system.

The errors in the model are associated with the modal truncation and the proximity of the calculation point to the flexible partition. These two factors have been studied for the system, using three different approximations including all the modes up to 400 Hz, 700 Hz and 1000 Hz, as indicated in Table 2.3 for each subsystem. The relationship between the natural frequency of the highest order mode included in the summation and the number of modes having natural frequencies below this value increases exponentially (Bullmore *et al.*, 1987).

Table 2.3. Number of modes included within the three different ranges of natural frequencies

Subsystem	Up to 400 Hz	Up to 700 Hz	Up to 1000 Hz
Source room	127	588	1584
Panel	15	28	41
Receiving room	151	695	1903

Figures 2.5 compares the results obtained for the acoustic impedance in the source and the receiving room as a function of the distance to the vibrating surface at a frequency of 156 Hz. The number of modes used in the simulation has been increased to include the total number in each frequency range for the three cases in Table 2.3. This is a normal frequency of the panel not coincident with any cavity resonances.

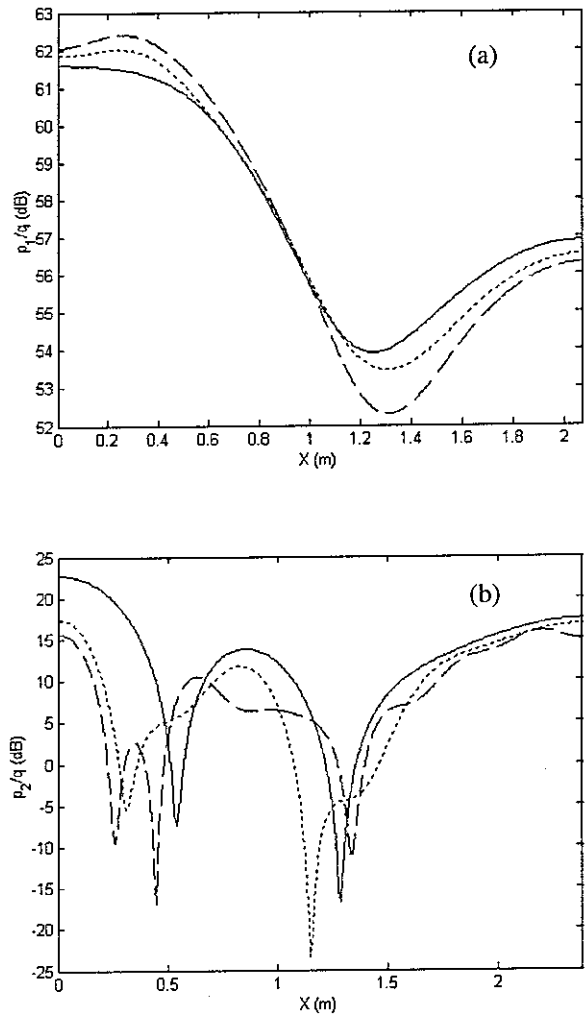

Figure 2.5. Acoustic impedance in (a) the source room and (b) the receiving room as a function of the distance to the partition calculated using the total number of modes up to 400 Hz (solid line), up to 700 Hz (dotted line) and up to 1000 Hz (dashed line), when the coupled system is excited at a frequency of 156 Hz

The general conclusion that is observed from the analysis of these figures is that, as it could be expected, the effect of modal truncation is more important in the receiving room, which is excited acoustically via the coupling with the partition, than in the source room. For the source room the total acoustic pressure field is dominated by the primary source, and the acoustic field as a function of the distance to the panel is similar to a standing wave through the enclosure. A similar behavior has been observed over the whole frequency range analysed, from 0 to 400 Hz. The truncated series of modal terms have converged to within a fraction of a decibel, and there are not significant differences between the near field and the far field.

For the receiving room, however, the pressure field as a function of the position changes considerably as we increase the number of modes used in the summation, presenting more near field features. Even when all the modes below 1000 Hz are included it can be observed that the modal approach has not yet converged: important differences still exist between the three approximations. This room is, then,

the most severe test of modal convergence. The same comparison for the truncated series up to 400 Hz and 700 Hz has been performed as a function of frequency for a near field position (1.5 cm from the panel) and a far field position (2 m from the panel). The results obtained are presented in Figure 2.6.

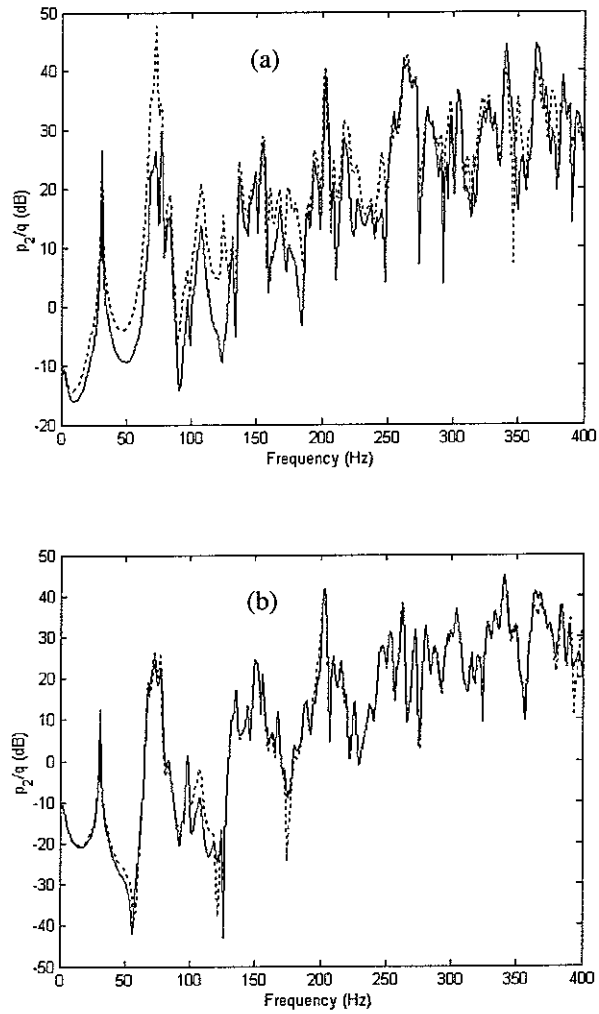

Figure 2.6. Acoustic impedance in the receiving room for (a) the near and (b) the far field, calculated using the total number of modes up to 400 Hz (solid line) and 700 Hz (dotted line)

As expected, the discrepancies are more important in the low frequency range and for the near field. The contribution of several modes can vary appreciably with the number of terms in the summation. To reach convergence, the modal superposition method must include an extremely high number of cavity modes, making the method impractical.

In an attempt to overcome this problem, the equivalent sources method has been investigated. The basis and the results obtained with this technique are explained in Appendix A. It is found to work very well for rigid boundary conditions, but similar convergence problems to those above appear when analysing mixed boundary conditions, i.e., rigid cavities and flexible partition. For the rest of the report the modal fully coupled model has been employed. This description should not be a problem in the source room, but it can lead to convergence mistakes in the receiving enclosure.

3. SOUND TRANSMISSION LOSS

The analytical model developed in the previous section will now be used to obtain an estimate of the sound transmission loss for the aluminium panel in three different situations: Case 1 corresponds to the sound transmission through the partition between the two reverberant rooms; case 2 corresponds to the sound transmission when the panel is coupled to the source room and radiating to free field and case 3 corresponds to the case where the partition is mounted in an infinite baffle. At the end of the section, the case of the panel in the free field and radiating to the receiving room is also presented.

The comparison of the results obtained with the simulations will allow us to characterise the effects from the individual modal behaviours in the two rooms and the structural modes of the partition. The analysis frequency range has been extended up to 600 Hz. All the results are presented for the fully coupled system and when using a total number of normal modes having natural frequencies below 700 Hz.

3.1 Aluminium partition in the transmission suite

The sound insulation characteristic of a wall is usually characterised in terms of a sound reduction index, R, expressed by (Egan, 1972; Beranek and Vér, 1992):

$$R(\omega) = 10\log_{10}\left(\frac{\Pi_{\text{inc}}(\omega)}{\Pi_{\text{trans}}(\omega)}\right) \quad \text{(dB)}, \tag{3.1}$$

where $\Pi_{\text{inc}}(\omega)$ = sound power incident on the wall at frequency ω;

$\Pi_{\text{trans}}(\omega)$ = sound power transmitted through the wall at frequency ω.

The sound reduction index typically depends on the angle of incidence of the impinging sound wave. However, in order to characterise the transmission of sound between the source and the receiving room, it is assumed that the sound is incident on the partition from all angles with approximately equal probability. If the sound fields in the two rooms are diffuse and provided the sound is transmitted only through the dividing wall, the sound intensity I_{random} (in W/m^2) is related to the space-average mean-square sound pressure in the source room $\langle p^2_{\text{source}} \rangle$ by:

$$I_{\text{random}} = \frac{\langle p^2_{\text{source}} \rangle}{4\rho_0 c_0}. \tag{3.2}$$

The sound power incident on the wall (in W) is given by

$$\Pi_{\text{inc}} = I_{\text{random}} S_p = \frac{\langle p^2_{\text{source}} \rangle S_p}{4\rho_0 c_0}. \tag{3.3}$$

The transmitted sound power (in W) is obtained from the power balance of the receiver room as

$$\Pi_{\text{trans}} = \frac{\langle p_{\text{rec}}^2 \rangle A_{\text{rec}}}{4\rho_0 c_0}. \tag{3.4}$$

The sound reduction index (in dB) may thus be evaluated from

$$R = L_{\text{source}} - L_{\text{rec}} + 10\log_{10}\left(\frac{S_p}{A_{\text{rec}}}\right), \tag{3.5}$$

where L_{source} = average sound pressure level in the source room;

L_{rec} = average sound pressure level in the receiving room;

S_p = area of the dividing wall;

A_{rec} = equivalent absorption area of the receiving room determined from reverberation measurements.

To characterise the panel sound transmission, the mean square sound pressure average in a number of positions through the cavities should be determined. We can relate this quantity to the total acoustic potential energy, E_p, given by (Nelson *et al.*, 1987):

$$E_p(\omega) = \frac{1}{4\rho_0 c_0^2}\int_V |p(x,y,z,\omega)|^2 \, dV, \tag{3.6}$$

where V is the volume of the room. If the acoustic pressure is expressed as a modal summation and the normal modes series constitute an orthogonal base, Eq. (3.6) can be written as:

$$E_p(\omega) = \frac{V}{4\rho_0 c_0^2}\sum_{lmn=0}^{\infty} |a_{lmn}(\omega)|^2, \tag{3.7}$$

leading to the following expression for the sound reduction index:

$$R = 10\log_{10}\left(\frac{E_{p\,\text{source}}}{E_{p\,\text{rec}}}\frac{V_{\text{rec}}}{V_{\text{source}}}\right) + 10\log_{10}\left(\frac{s_p}{\overline{\alpha}_{\text{rec}}\, 2\cdot(s_{x\,\text{rec}} + s_{y\,\text{rec}} + s_{z\,\text{rec}})}\right) \quad (dB), \tag{3.8}$$

where $\overline{\alpha}_{\text{rec}}$ is the average absorption coefficient of the receiving walls, assumed independent of frequency (Eq. (2.23)).

This expression has been used in the computer simulations to calculate R for the aluminium partition in the transmission suite described above. The results obtained are presented in Figure 3.1, showing the total potential energy in the source and the receiving room, and the sound reduction index for the panel. As it can be observed, there are two distinct regions, the low modal density zone, where the modal characteristics of the rooms are clearly visible, and in the high modal overlap frequency range, above 400 Hz approximately.

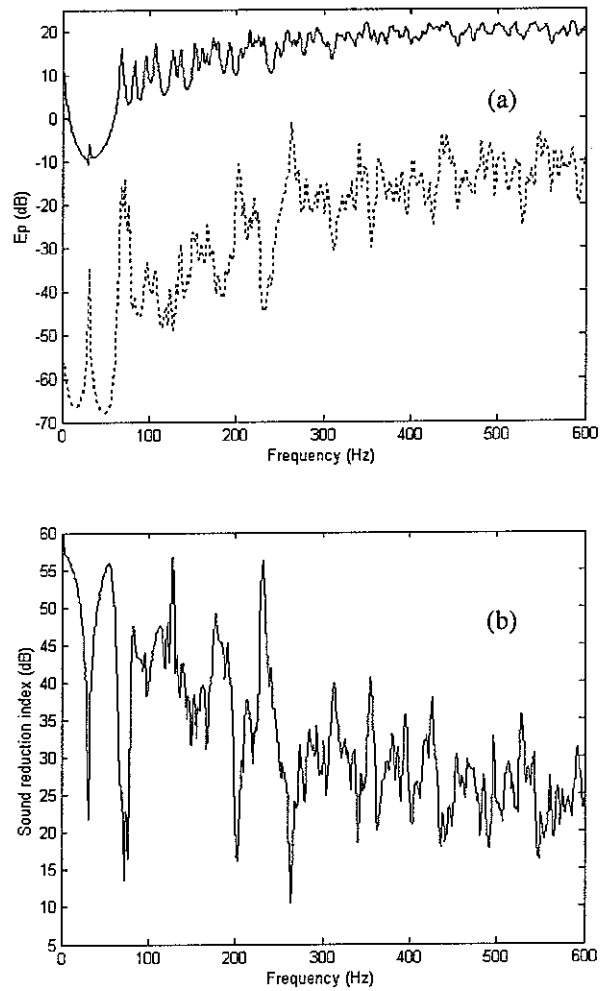

Figure 3.1. (a) Total acoustic potential energy in the source room (solid line) and in the receiving room (dotted line). (b) Calculated sound reduction index as a function of frequency for the aluminium panel in the sound transmission suite

3.2 Aluminium partition coupled with one cavity

A schematic representation of the physical set-up analysed in this section is shown in Figure 3.2. The aluminium partition is excited by the loudspeaker in the source room and radiates to the free field. The situation for the source room has not changed with respect to the previous section, and the sound power incident on the wall can again be calculated from Eq. (3.3).

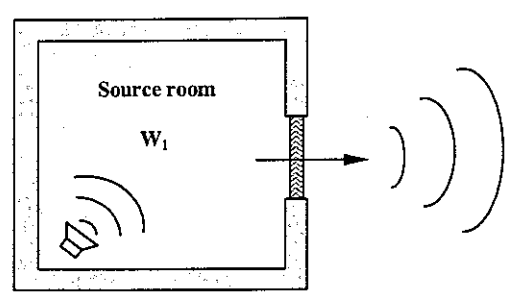

Figure 3.2. Aluminium partition connected to one cavity

The total acoustic power generated by the panel can be calculated as the sum of the squared moduli of each structural mode amplitude multiplied by its self-radiation resistance, and the sum of the cross products of the structural mode amplitudes multiplied by their mutual-radiation resistance (Cunefare, 1991; Baumann et al., 1991). The acoustic power output as a single frequency can be expressed as:

$$\Pi_{\text{trans}} = \mathbf{a}^{(p)^{\mathrm{H}}} \mathbf{M} \mathbf{a}^{(p)}, \tag{3.9}$$

where $\mathbf{M}$ is a real, symmetric, positive definite matrix in which the diagonal terms are the self-radiation resistances and the off-diagonal terms are the mutual-radiation resistances. The values of this matrix are calculated integrating the far-field intensity over a hemisphere surrounding the plate. Cunefare (1991) has undertaken this integral numerically.

The approach followed in this report uses the formulation in terms of amplitudes of an array of elemental radiators (Elliott and Johnson, 1993; Johnson, 1996). If the vector of complex linear velocities of each of these elemental sources at a single frequency is denoted $\mathbf{v}$, the vector of complex acoustic pressures immediately in front of each source, $\mathbf{p}$, is given by:

$$\mathbf{p} = \mathbf{Z}\mathbf{v}, \tag{3.10}$$

in which $\mathbf{Z}$ is a matrix of acoustic impedances. The acoustic power radiated by this array of elemental sources is proportional to the real part of the sum of the conjugate volume velocities of each radiator multiplied by the corresponding acoustic pressure. It reads:

$$\Pi_{trans} = \frac{s}{2}\mathrm{Re}\left[\mathbf{v}^{H}\mathbf{p}\right], \tag{3.11}$$

where s is the surface of the elemental radiators, assumed to be of equal size. Using Eq. (3.10), the acoustic power output can then be expressed as:

$$\Pi_{\text{trans}} = \frac{s}{2}\mathrm{Re}\left[\mathbf{v}^{\mathrm{H}}\mathbf{Z}\mathbf{v}\right] = \frac{s}{4}\mathbf{v}^{\mathrm{H}}[\mathbf{Z}+\mathbf{Z}^{\mathrm{H}}]\mathbf{v} = \mathbf{v}^{\mathrm{H}}\mathbf{R}\mathbf{v}, \tag{3.12}$$

where the symmetry of $\mathbf{Z}$ has been used, and the matrix $\mathbf{R}$ is defined as:

$$\mathbf{R} = \frac{s}{2}\mathrm{Re}[\mathbf{Z}]. \tag{3.13}$$

If the radiating surface is plane and in an infinite baffle, the terms of this radiation resistance matrix may be calculated analytically. The specific acoustic transfer impedance from an elementary radiator at position $\mathbf{y}$ to an observation position $\mathbf{x}$ is given by (Vitiello *et al.*, 1989)

$$z(\mathbf{x},\mathbf{y}) = \frac{p(\mathbf{y})}{v(\mathbf{x})} = \frac{\mathrm{j}\omega\rho s}{2\pi r}\mathrm{e}^{-\mathrm{j}kr} \tag{3.14}$$

in which r is the distance between the observation position and the elemental radiator.

The vector of complex linear velocities at the positions of the I elemental radiators can be written as:

$$\mathbf{v} = \boldsymbol{\varphi}\mathbf{a}^{(p)}, \tag{3.15}$$

in which the elements of the matrix $\boldsymbol{\varphi}$ are the panel normal modes evaluated in the positions of the elementary radiators, which have been deduced previously. The total sound power radiated by the structure, after substituting Eq. (3.15) into Eq. (3.12):

$$\Pi_{\text{trans}} = \mathbf{v}^{\mathrm{H}}\mathbf{R}\,\mathbf{v} = \mathbf{a}^{(p)\mathrm{H}}\boldsymbol{\varphi}^{H}\mathbf{R}\,\boldsymbol{\varphi}\mathbf{a}^{(p)} \tag{3.16}$$

The acoustic power radiated by the aluminium panel has been calculated using this method. The number of elemental radiators has been progressively increased until no significant differences were found. The final number used was 20 elementary radiators along both its length and its width. The matrix of radiation resistances for an array of I elementary radiators in an infinite baffle is given by (Elliott and Johnson, 1993)

$$\mathbf{R} = \frac{\omega^2 \rho S^2}{4\pi c}\begin{bmatrix} 1 & \frac{\sin(k r_{12})}{k r_{12}} & \cdots & \frac{\sin(k r_{1I})}{k r_{1I}} \\ \frac{\sin(k r_{21})}{k r_{21}} & 1 & & \\ \cdots & \cdots & \cdots & \cdots \\ \frac{\sin(k r_{I1})}{k r_{I1}} & & & 1 \end{bmatrix} \tag{3.17}$$

in which r_{ij} is the distance from element i to element j.

The results obtained for the sound reduction index are presented in Figure 3.3 as a function of frequency. Although some modal contributions have disappeared due to the removal of the receiving room, the modal behaviour of the source room in the low frequency range is clearly observed.

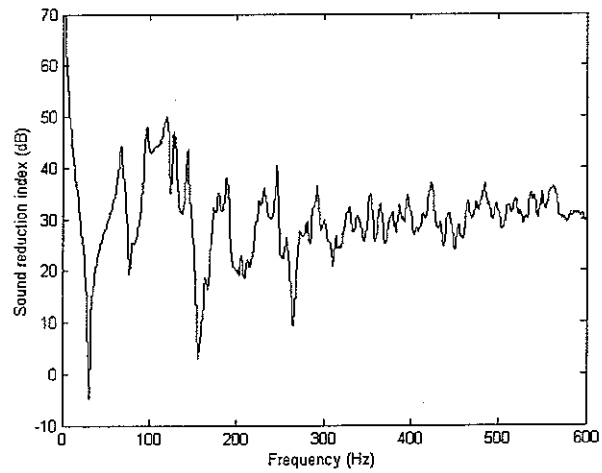

Figure 3.3. Sound reduction index as a function of frequency for the aluminium panel radiating to free field

3.3 Aluminium partition mounted in an infinite baffle

The geometry of the problem studied under this section is illustrated in Figure 3.4. The aluminium partition is situated in an infinite baffle, and is excited by a diffuse sound field.

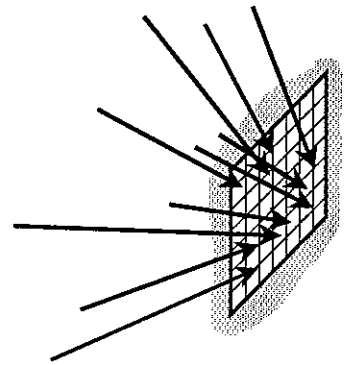

Figure 3.4. Aluminium partition mounted in an infinite baffle

The diffuse sound field can be considered as an infinite number of propagating waves with random phase relations, arriving from uniformly distributed directions and with the propagation vector pointing toward the plate (Pierce, 1981). Garcia-Bonito (Garcia-Bonito, 1996) has used two possible forms for the diffuse field pressure on an arbitrary plane x-y, in which either the real and imaginary parts of the complex pressure are randomly distributed, or the modulus of the incoming wave is assumed constant and the relative phase is randomly distributed, i.e.,

$$p_{\text{diff}}(x,y) = \sum_{K=1}^{K_{\max}} \sum_{L=1}^{L_{\max}} (a_{KL} + jb_{KL}) \sin\theta_K \mathrm{e}^{\mathrm{j}k(x\sin\theta_K\cos\phi_L + y\sin\theta_K\sin\phi_L)} \tag{3.18}$$

$$p_{\text{diff}}(x,y) = \sum_{K=1}^{K_{\max}} \sum_{L=1}^{L_{\max}} z\mathrm{e}^{\mathrm{j}\varphi_{KL}} \sin\theta_K \mathrm{e}^{\mathrm{j}k(x\sin\theta_K\cos\phi_L + y\sin\theta_K\sin\phi_L)} \tag{3.19}$$

Both equations represent the pressure in the x-y plane due to a combination of $L_{\max}$ plane waves in the azimuthal direction (corresponding to azimuthal angles $\phi_L = 2\pi L / L_{\max}, L = 1,2,...,L_{\max}$) for each of the $\pi / K_{\max}$ vertical incident directions (corresponding to polar angles $\theta_K = K\pi / K_{\max}$, $L = 1,2,...,K_{\max}$). The values of a_{KL} and b_{KL} are chosen from a random population with Gaussian distribution N(0,1) and the multiplicative factor $\sin\theta_K$ is included to ensure that, on average, the energy associated with the incident waves was uniform from all directions. The value of φ_{KL} is chosen from a random population with uniform distribution and z is a constant complex number.

The model of a diffuse field used in this work corresponds to the stochastic approach described above, given by Eq. (3.18). The double summation was truncated in practice at $K_{\max} = 8$ and $L_{\max} = 32$, defining a set of 256 plane waves per sample of diffuse field, each of them is unaffected by any form of diffraction or reflection in the space domain where the model is applied. In order to test whether the

diffuse field generated by Eq. (3.18) was a reasonable approximation to an ideal diffuse field, the spatial cross-correlation function was computed using the expression

$$\frac{\left\langle p_p(x_0)\, p_p^*(x_0+\Delta x)\right\rangle}{\left\langle \left|p_p(x_0)\right|^2 \right\rangle}, \tag{3.20}$$

where $\langle\ \rangle$ denotes spatial average. Figure 3.5 shows a comparison the theoretically value, given by

$$\frac{\sin(k|\Delta x|)}{k|\Delta x|}. \tag{3.21}$$

and the predicted value given by Eq. (3.20), averaging over 400 samples of different diffuse sound field. One can see that the agreement between the model and the theory is satisfactory, which indicates that Eq. (3.18) is a valid model of a 3D diffuse acoustic field.

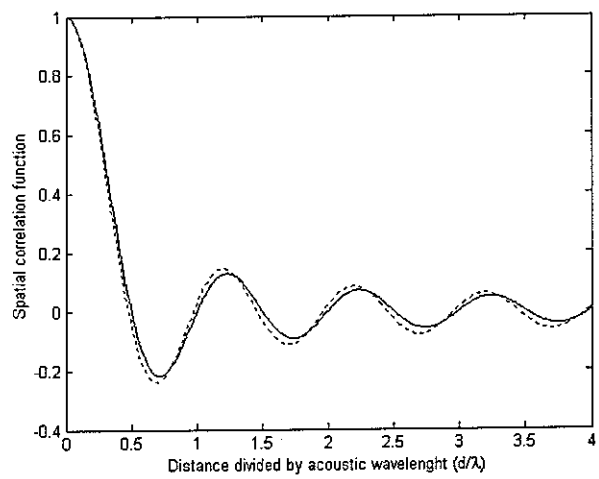

Figure 3.5. Spatial correlation function obtained with the theoretical expression for a diffuse pressure field (solid line) and due to a number of uniformly distributed plane waves (dotted line)

For the calculation of the incident sound power, each incident plane wave can be described as

$$p_{\mathrm{inc}(\theta,\varphi)} = P_{\mathrm{inc}} e^{j\omega t - jk(x\sin\theta\cos\phi + y\sin\theta\sin\phi + z\cos\theta)}. \tag{3.22}$$

and the power due to a plane wave is given by:

$$\Pi_{\mathrm{inc}(\theta,\varphi)} = \frac{1}{2}\mathrm{Re}\left[\int_{S_p} p_{\mathrm{inc}(\theta,\varphi)}\, \mathbf{v}^*_{\mathrm{inc}(\theta,\varphi)} \cdot \mathbf{n}\, dS\right] = \frac{|P_{\mathrm{inc}}|^2 S_p}{2\rho_0 c_0}\cos\theta, \tag{3.23}$$

in which $\mathbf{v}_{(\theta,\varphi)}$ is the incident acoustic velocity and $\mathbf{n}$ is the unit normal vector to the plate.

The acoustic power radiated by the plate due to this incident wave only is:

$$\Pi_{\mathrm{trans}(\theta,\phi)} = \frac{1}{2}\mathrm{Re}\left[\int_{S_p} p_{(\theta,\varphi)}\, \mathbf{v}^*_{(\theta,\phi)} \cdot \mathbf{n}\, dS\right], \tag{3.24}$$

in which $p_{(\theta,\varphi)}$ is the acoustic pressure radiated by the plate, and $\mathbf{v}_{(\theta,\phi)} \cdot \mathbf{n}$ is its normal velocity.

The integral in Eq. (3.24) can be approximated by assuming that the sound radiated by the plate is due to a number of elementary radiators covering the plate, with the partition discretisation described in Section 2.4.2:

$$\Pi_{\text{trans}(\theta,\phi)} = \frac{S}{2}\text{Re}\left[\mathbf{v}^{\text{H}}\mathbf{Z}\,\mathbf{v}\right] = \mathbf{v}^{\text{H}}\mathbf{R}\,\mathbf{v} = \mathbf{a}^{(p)^{\text{H}}}\boldsymbol{\varphi}^{\text{H}}\mathbf{R}\,\boldsymbol{\varphi}\,\mathbf{a}^{(p)} \tag{3.25}$$

in which the elements of the matrix $\boldsymbol{\varphi}$ are the panel normal modes evaluated in the positions of the elementary radiators and the matrix $\mathbf{R}$ of radiation resistances is given by Eq. (3.17).

The elements of the vector $\mathbf{a}^{(p)}$ are the complex modal amplitudes when the panel is excited by an obliquely incident plane wave. They have the following expression (Fuller *et al.*, 1996):

$$a_{qr}^{(p)} = \frac{2\left|P_{\text{inc}}\right|\omega I_q I_r}{\text{j}m[\omega^2 - (1+\text{j}\eta)\omega_{qr}^2)]} \tag{3.26}$$

where the factors I_q and I_r are given by:

$$I_q = \begin{cases} \dfrac{-\text{j}}{2}\text{sgn}(\sin\theta\cos\varphi) & \text{if } (q\pi)^2 = [\sin\theta\cos\varphi\,(\omega b_p / c)]^2 \\ \dfrac{q\pi\left\{1-(-1)^q\exp[-\text{j}\sin\theta\cos\varphi\,(\omega b_p / c)]\right\}}{(r\pi)^2 - [\sin\theta\cos\varphi\,(\omega b_p / c)]^2} & \text{if } (q\pi)^2 \neq [\sin\theta\cos\varphi\,(\omega b_p / c)]^2 . \end{cases} \tag{3.27}$$

and

$$I_r = \begin{cases} \dfrac{-\text{j}}{2}\text{sgn}(\sin\theta\sin\varphi) & \text{if } (r\pi)^2 = [\sin\theta\sin\varphi\,(\omega c_p / c)]^2 \\ \dfrac{r\pi\left\{1-(-1)^r\exp[-\text{j}\sin\theta\sin\varphi\,(\omega c_p / c)]\right\}}{(r\pi)^2 - [\sin\theta\sin\varphi\,(\omega c_p / c)]^2} & \text{if } (r\pi)^2 \neq [\sin\theta\sin\varphi\,(\omega c_p / c)]^2 . \end{cases} \tag{3.28}$$

The incident and radiated diffuse field are then obtained through integration over a hemisphere surrounding the plate (Panneton and Atalla, 1996; Sgard et al., 2000). They take the form:

$$\Pi_{\text{inc}}^{\text{d}} = \int_0^{2\pi}\int_0^{\pi/2}\Pi_{\text{inc}(\theta,\phi)}\sin\theta\,\text{d}\theta\,\text{d}\phi \tag{3.29}$$

$$\Pi_{\text{trans}}^{d} = \int_0^{2\pi}\int_0^{\pi/2}\Pi_{\text{trans}(\theta,\phi)}\sin\theta\,\text{d}\theta\,\text{d}\phi . \tag{3.30}$$

These integral are approximated by the sum of a sufficient number of plane waves uniformly distributed over the half space. The calculation of the acoustic power radiated by the system is then required for each plane wave defined by the angle (θ,φ) and the complex amplitude P_{inc}, to yield to the acoustic power radiated in the case of a diffuse field excitation. The response due to the superposition of all the plane waves is simply the sum of the contribution due to each one, both for the incident and transmitted sound power.

A total number of 256 plane waves has been used in the simulation of the diffuse field, after verifying that taking a higher number does not significantly affect the result. In Figure 3.6 the sound reduction index obtained for the aluminium panel is compared with the prediction given by the field incident mass law (Fahy, 1985):

$$R_f = 20\log_{10}(mf) - 47 \quad (\text{dB}), \tag{3.31}$$

and with the one obtained when considering one single 45° incident plane wave.

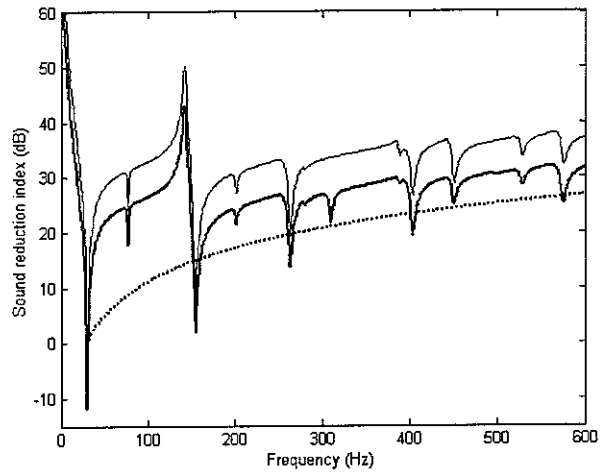

Figure 3.6. Sound reduction index corresponding to an aluminium panel in an infinite baffle for diffuse field excitation (bold) and for a 45° incident plane wave (solid) compared with the mass law prediction (dotted)

The first modal frequencies with the corresponding modal indices up to 600 Hz are listed in Table 3.1. These can be identified with the peaks and dips of the sound reduction index in the Figure 3.6.

Table 3.1. Modal indices and natural frequencies for the aluminium panel up to 600 Hz

Modal indices		Normal frequencies (Hz)
1	1	31.1282
1	2	77.8206
2	1	77.8206
2	2	124.5130
1	3	155.6412
3	1	155.6412
2	3	202.3335
3	2	202.3335
1	4	264.5900
4	1	264.5900
3	3	280.1541
2	4	311.2824
4	2	311.2824
3	4	389.1030
4	3	389.1030
1	5	404.6671
5	1	404.6671
2	5	451.3595
5	2	451.3595
4	4	498.0518
3	5	529.1800
5	3	529.1800
1	6	575.8724
6	1	575.8724

It is observed that as we increase the frequency, the agreement with the mass law gets better, but the values obtained with the numerical simulation in this range are around 5 dB higher than the mass law prediction. The results are also shown for a single 45° incident plane wave. As the diffuse field is able to excite the panel normal modes more uniformly, the sound power radiated is higher and the sound reduction index is below the value calculated for the single plane. Excepting for a correction factor, the two graphs for this incident angle are very similar, as it has been already pointed out by Fahy (1985).

A summary of the results obtained for the sound reduction index in narrowband and third octave band is presented in Figure 3.7, in which the modal behaviour of the cavities in the low modal density region is clearly seen. The Schroeder frequency for the source and receiving room is situated around 400 and 450 Hz respectively. Above this value, in the high modal overlap frequency range, the three different results converge towards the same value.

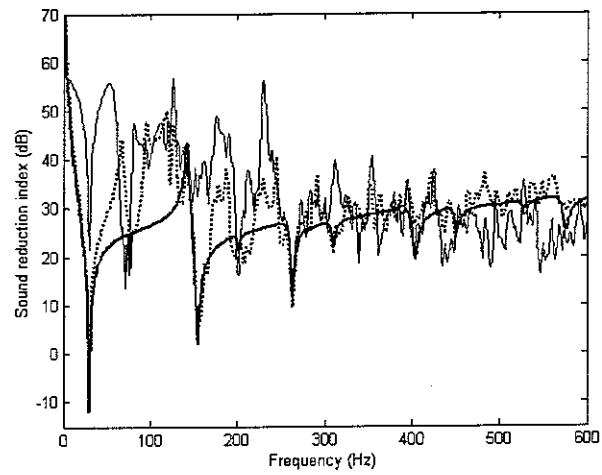

Figure 3.7. Sound reduction index as a function of frequency for the aluminium panel calculated in the sound transmission suite (solid), radiating to free space (dotted) and mounted in an infinite baffle (thick) when there is one loudspeaker in the source room

3.4 Aluminium partition coupled to the receiving room alone

This report is presenting a signal processing formulation for the reproducing a diffuse acoustic pressure field using an array of loudspeakers in the source room. It would be, then, interesting to study the variation of the sound reduction index for the aluminium partition once the modal characteristics of the first cavity has been removed. This is equivalent to consider the panel coupled to the receiving room only, and excited by a pure diffuse pressure field.

A schematic representation of the physical set-up analysed is shown in Figure 3.8. The aluminium partition is excited in the way described in the previous section, with the pressure field generated by a superposition of planes waves, and radiates to the receiving room.

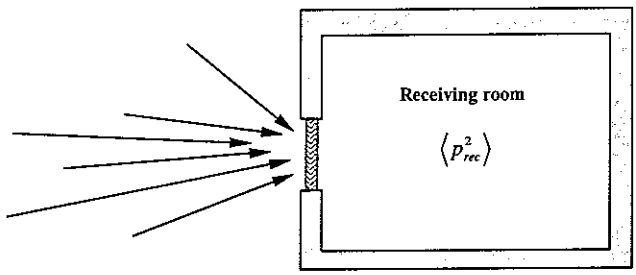

Figure 3.8. Aluminium partition connected to the receiving room only

In this case it is necessary to reformulate the theoretical description of the panel-cavity coupled configuration to account for the diffuse field excitation in free field. The system of Eqs. (2.29-2.31), used to describe the behaviour of the cavity-panel-cavity coupled system, have to be modified for the panel-receiving room configuration as:

$$a_{qr}^{(p)} = \frac{\omega}{\mathrm{j}m[\omega^2 - (1+\mathrm{j}\eta)\omega_{qr}^2]}\left(2\left|P_{\mathrm{inc}}\right| I_q I_r - \frac{1}{S_p}\sum_{l_2 m_2 n_2=0}^{\infty} a_{l_2 m_2 n_2}^{(2)} G_{l_2 m_2 n_2, qr}^{(2)}\right) \tag{3.32}$$

$$a_{l_2 m_2 n_2}^{(2)} = \frac{\rho_0 c_0^2 \omega}{V_2[2B_{l_2 m_2 n_2}\omega + \mathrm{j}(\omega^2 - \omega_{l_2 m_2 n_2}^2)]}\left(\sum_{qr=1}^{\infty} a_{qr}^{(p)} G_{l_2 m_2 n_2, qr}^{(2)}\right). \tag{3.33}$$

where the equation for the panel has been modified to include the modal terms when the panel is excited by one obliquely incident plane wave instead of the coupling with the source room. The factors I_q and I_r are given by Eqs. (3.27) and (3.28) respectively.

Substituting now the modal panel amplitudes, Eq. (3.32), into the expression for the receiving room, Eq. (3.33), we obtain:

$$\begin{aligned} a_{l_2 m_2 n_2}^{(2)} = & \frac{\rho_0 c_0^2 \omega}{V_2[2B_{l_2 m_2 n_2}\omega + \mathrm{j}(\omega^2 - \omega_{l_2 m_2 n_2}^2)]} \\ & \times\left[\sum_{qr=1}^{\infty} \frac{\omega}{\mathrm{j}m[\omega^2 - (1+\mathrm{j}\eta)\omega_{qr}^2)]}\left(2\left|P_{\mathrm{inc}}\right| I_q I_r - \frac{1}{s_p}\sum_{l_2' m_2' n_2'=0}^{\infty} a_{l_2' m_2' n_2'}^{(2)} G_{l_2' m_2' n_2', qr}^{(2)}\right) G_{l_2 m_2 n_2, qr}^{(2)}\right]. \end{aligned} \tag{3.34}$$

After rearrangement, it reads:

$$\frac{V_2[2B_{l_2m_2n_2}\omega+\mathrm{j}(\omega^2-\omega_{l_2m_2n_2}^2)]}{\rho_0 c_0^2\omega}a_{l_2m_2n_2}^{(2)}+\sum_{qr=1}^{\infty}\sum_{l_2'm_2'n_2'=0}^{\infty}\frac{\omega}{jms_p[\omega^2-(1+\mathrm{j}\eta)\omega_{qr}^2)]}G_{l_2'm_2'n_2',qr}^{(2)}G_{l_2m_2n_2,qr}^{(2)}a_{l_2'm_2'n_2'}^{(2)}$$
$$=\sum_{qr=1}^{\infty}\frac{2|P_{\mathrm{inc}}|\omega I_q I_r}{jm[\omega^2-(1+\mathrm{j}\eta)\omega_{qr}^2)]}G_{l_2m_2n_2,qr}^{(2)}\,. \tag{3.35}$$

This equation can be expressed in matrix form as:

$$\mathbf{Z}_2\mathbf{a}^{(2)}=\mathbf{Z}_w^{(2)} \tag{3.36}$$

where $\mathbf{Z}_2$ is the $(N^{(2)}\times N^{(2)})$ matrix defined by

$$Z_{l_2m_2n_2,l_2'm_2'n_2'}=\begin{cases}\sum_{qr=1}^{\infty}A_{qr}^{(p)}\,G_{l_2'm_2'n_2',qr}^{(2)}G_{l_2m_2n_2,qr}^{(2)} & \text{if } l_2'm_2'n_2'\neq l_2m_2n_2,\\ \sum_{qr=1}^{\infty}A_{qr}^{(p)}\,G_{l_2'm_2'n_2',qr}^{(2)}G_{l_2m_2n_2,qr}^{(2)}+\dfrac{V_1[2B_{l_2m_2n_2}\omega+\mathrm{j}(\omega^2-\omega_{l_2m_2n_2}^2)]}{\rho_0c_0^2\omega} & \text{otherwise}\end{cases} \tag{3.37}$$

and $\mathbf{Z}_w^{(2)}$ is the matrix due to one incident plane wave, with dimensions $(N^{(1)}\times 1)$, whose elements are defined in Eq. (3.35).

These equations have been implemented in a Matlab program for the comparison with the sound reduction index in free field. These are the results (Figure 3.9) we could expect after removing the modal contribution of the source room via an array of near-field loudspeakers.

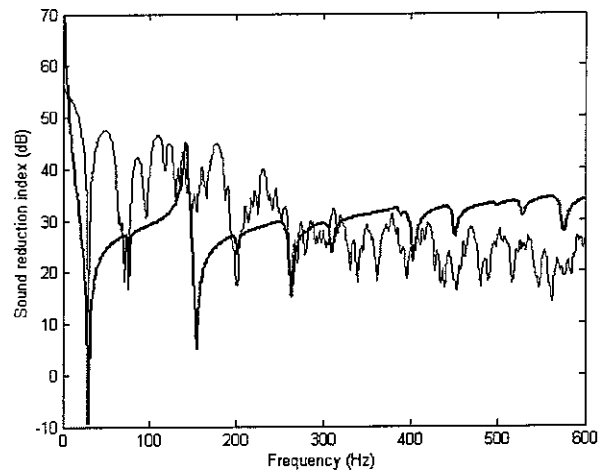

Figure 3.9. Sound reduction index as a function of frequency for the aluminium panel coupled to the receiving room only (dotted) and radiating into free space (solid)

4. THE REPRODUCTION OF A DIFFUSE FIELD WITH AN ARRAY OF LOUDSPEAKERS

The problem of simulating a pressure field having the same statistical properties than a diffuse field using an array of loudspeakers is analysed in this section. Using the analytical solutions presented before, the sound reduction index is calculated for the three different configurations: in the transmission suite, with the partition coupled to the source room, and with the panel mounted in an infinite baffle.

The signal processing formulation proposed is the same for the three cases. We consider an array of evenly spaced microphones situated over the plate surrounded by a rigid baffle. The microphone outputs provide a measure of the spatial variation of the pressure field, which ideally corresponds to that of a diffuse field, $\mathbf{d}$. This can be assumed to be derived from a set of uncorrelated white unit variance reference signals, $\mathbf{x}$, via a matrix of filters $\mathbf{D}$, as illustrated in Figure 4.1.

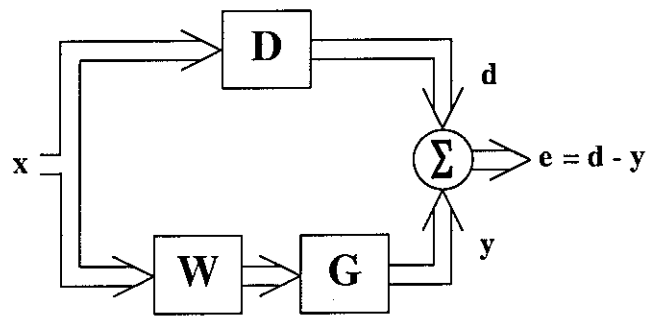

Figure 4.1. Block diagram for the calculation of the least-squares control filter

The matrix of control filters, $\mathbf{W}$, is adjusted to determine the optimum input signals to an array of loudspeakers, which drive the sensor outputs, $\mathbf{y}$, via the matrix of plant responses, $\mathbf{G}$ (Elliott, 2000; Elliott *et al.*, 2001). The vector of error signals at a given frequency is thus defined to be

$$\mathbf{e} = \mathbf{d} - \mathbf{y} = (\mathbf{D} - \mathbf{G}\,\mathbf{W})\mathbf{x}. \tag{4.1}$$

For the cost function to be optimised a mean-squared error criteria has been chosen as the sum of the squared error signals normalised by the sum of the squared signals due to the diffuse field. Using the fact that the reference signals are uncorrelated, so that $\mathbf{S}_{xx} = \mathbf{I}$, the optimal least-squares matrix of filters is given by (Elliott, 2000; Elliott *et al.*, 2001)

$$\mathbf{W}_{opt} = [\mathbf{G}^{\mathrm{H}}\mathbf{G}]^{-1}\mathbf{G}^{\mathrm{H}}\mathbf{D} = \mathbf{G}^{\dagger}\mathbf{D}, \tag{4.2}$$

where $\mathbf{G}^{\dagger}$ is the pseudo-inverse of $\mathbf{G}$.

Once the matrix of filters driven the loudspeakers has been optimised, the reproduction of the sound reduction index can be analysed.

4.1 Aluminium partition mounted in an infinite baffle in the free field

4.1.1 Analytical expressions

The expression for the structural velocity at a point $\mathbf{r}_p$ on the panel in terms of the normal modes has been presented previously in Eq. (2.7), as

$$v(\mathbf{r}_p,\omega)=\sum_{s=1}^{\infty} a_s^{(p)}(\omega)\phi_s(\mathbf{r}_p), \tag{4.3}$$

where $a_s^{(p)}(\omega)$ is the complex amplitude of the s-th structural mode, defined in this case as

$$a_s^{(p)}(\omega)=\frac{\omega}{\mathrm{j}M_s^{(p)}[\omega^2-(1+\mathrm{j}\eta)\omega_s^2)]}\int_{S_p} p(\mathbf{r}_p)\phi_s^{(p)}\,\mathrm{d}S\ , \tag{4.4}$$

in which p is the pressure field generated by the loudspeakers. This integral can be approximated using the formulation in terms of the elemental radiators covering the plate with the discretisation described previously. Eq. (4.4) can be written in matrix form as:

$$\mathbf{a}^{(p)}=\mathbf{R}_p\mathbf{P}=\mathbf{R}_p\mathbf{G}\mathbf{W}, \tag{4.5}$$

where $\mathbf{R}_p$ is the matrix of the modal terms multiplied by the normal panel modes evaluated at the positions of the elemental radiators, and $\mathbf{G}$ is the transfer function between the loudspeakers and the microphones over the panel, corresponding to the free field in this case.

The acoustic power output at a single frequency is given by Eq. (3.9), and substituting the value for the modal panel amplitudes, Eq. (4.5), we have

$$\Pi_{\text{trans}}=\mathbf{a}^{(p)\mathrm{H}}\mathbf{M}\mathbf{a}^{(p)}=(\mathbf{R}_p\mathbf{P})^{\mathrm{H}}\mathbf{M}\mathbf{R}_p\mathbf{P}, \tag{4.6}$$

where the matrix of modal radiation resistances is equal to

$$\mathbf{M}=\boldsymbol{\varphi}^{\mathrm{H}}\mathbf{R}\boldsymbol{\varphi}. \tag{4.7}$$

The minimum normalised mean-squared error signals has been shown to be (Elliott *et* al., 2001):

$$J_e(\mathbf{W}_{\text{opt}})=\frac{\mathrm{Tr}\left[(\mathbf{I}-\mathbf{G}\mathbf{G}^{\dagger})\mathbf{S}_{dd}\right]}{\mathrm{Tr}\left[\mathbf{S}_{dd}\right]}, \tag{4.8}$$

in which $\mathbf{S}_{dd}$ is the spectral density matrix generated at the microphones by the diffuse field, given by

$$\mathbf{S}_{dd}(\mathbf{r},\omega)=\mathbf{S}_{pp}(\omega)\frac{\sin k_0\mathbf{r}}{k_0\mathbf{r}}, \tag{4.9}$$

where $\mathbf{S}_{pp}(\omega)$ is the power spectral density at any point, which has been taken as unity, k_0 is the acoustic wavenumber and $\mathbf{r}$ is the separation distance between two measurement points. The matrix $\mathbf{D}$ is derived from an eigenanalysis of the matrix $\mathbf{S}_{dd}$.

The incident power over the panel due to a pure diffuse field has been calculate using the expression (Fahy, 1985):

$$\Pi_{\text{inc}} = \frac{\text{Tr}(\mathbf{S}_{dd})}{4\rho c}, \tag{4.10}$$

and the same form has been used to calculated the incident power for the diffuse pressure field generated by the loudspeakers, using the approximate spectral density matrix, which takes the form:

$$\mathbf{S}_{ddl} = \mathbf{G}\mathbf{G}^{\dagger}\mathbf{S}_{dd}(\mathbf{G}\mathbf{G}^{\dagger})^{\text{H}}. \tag{4.11}$$

We can also define the normalised mean-square error signals induced on the vibrating response of the panel when subjected to the diffuse pressure field generated by the array of loudspeakers. The spectral density matrix for the velocity response, using Eqs. (4.3) and (4.5), is given by

$$\mathbf{S}_{vv} = \boldsymbol{\varphi}^{(p)}\mathbf{R}_p\mathbf{S}_{ddl}(\boldsymbol{\varphi}^{(p)}\mathbf{R}_p)^{\text{H}}. \tag{4.12}$$

The mean-square error for the panel response is

$$J_{vv}(\mathbf{W}_{\text{opt}}) = \frac{\text{Tr}\left[\boldsymbol{\varphi}^{(p)}\mathbf{R}_p\mathbf{S}_{ee}(\mathbf{W}_{\text{opt}})(\boldsymbol{\varphi}^{(p)}\mathbf{R}_p)^{\text{H}}\right]}{\text{Tr}\left[\boldsymbol{\varphi}^{(p)}\mathbf{R}_p\mathbf{S}_{dd}(\boldsymbol{\varphi}^{(p)}\mathbf{R}_p)^{\text{H}}\right]}, \tag{4.13}$$

in which $\mathbf{S}_{ee}(\mathbf{W}_{\text{opt}})$ is the spectral density matrix of the error signal for the optimal control filter matrix, which has the expression

$$\mathbf{S}_{ee}(\mathbf{W}_{opt}) = \left[\mathbf{I} - \mathbf{G}\mathbf{G}^{\dagger}\right]\mathbf{S}_{dd}\left[\mathbf{I} - (\mathbf{G}\mathbf{G}^{\dagger})^{H}\right]. \tag{4.14}$$

Finally, we can define the normalised mean-square error signals induced on the radiated power by the panel when subjected to the diffuse pressure field generated by the array of loudspeakers. The spectral density matrix for the radiated power is given by

$$\mathbf{S}_{ww} = \mathbf{S}_{ddl}\mathbf{R}_p^{\text{H}}\mathbf{M}\mathbf{R}_p. \tag{4.15}$$

The mean-square error for the power radiated can be defined as

$$J_{ww}(\mathbf{W}_{\text{opt}}) = \frac{\text{Tr}\left[\mathbf{S}_{ee}(\mathbf{W}_{\text{opt}})\mathbf{R}_p^{\text{H}}\mathbf{M}\mathbf{R}_p\right]}{\text{Tr}\left[\mathbf{S}_{dd}\mathbf{R}_p^{\text{H}}\mathbf{M}\mathbf{R}_p\right]}. \tag{4.16}$$

4.1.2 Numerical simulations

To examine the feasibility of this method of reproducing a diffuse pressure field a series of numerical simulations have been performed, in which the error in the excitation, in the velocity response of the

panel and in the radiated power have been calculated using Eqs. (4.8), (4.13) and (4.16) respectively. An array of 20 x 20 uniformly spaced microphones situated over the panel has been exposed to the pressure field generated by an array of 2 x 2 loudspeakers, whose outputs are calculated according to Eq. (4.2). An illustration of the system is presented in Figure 4.2.

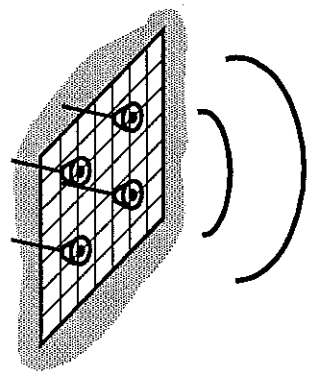

Figure 4.2. Four-loudspeakers array acting over the panel

Figure 4.3 shows the variation of the mean-square errors as a function of the frequency when the separation distance between the actuators and the panel has been taken as half that between the loudspeakers in the array. The error in the reproduction of the diffuse fields gets worse as the frequency increases, showing a smooth variation over the whole range. If we assume that a 10 dB reduction in the error constitutes a reasonable approximation for the simulation, the array of 2 x 2 loudspeakers is then sufficient to provide good results up to approximately 300 Hz. Figure 4.4 shows the minimum number of loudspeakers for a 10 dB reduction in the mean-square excitation error as a function of frequency. The same trend appears for the panel velocity and the radiated power but the modal characteristics are clearly visible in this case, although, as we intended to reproduce the excitation, the peaks and dips cannot be directly identified with resonances and antiresonances of the panel.

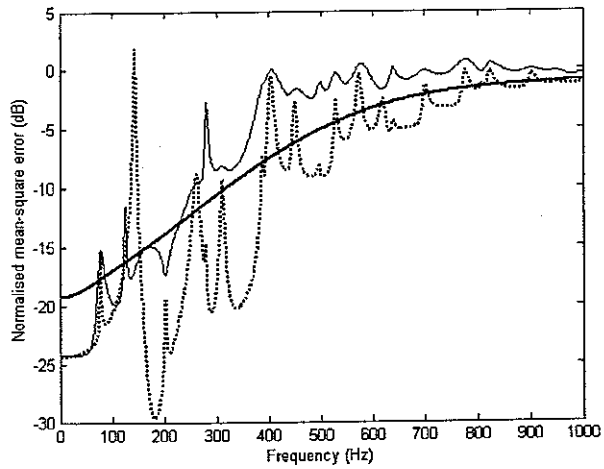

Figure 4.3. Normalised mean-square error associated with the approximate diffuse field using an array of four loudspeakers in the excitation (bold line), the velocity response (solid line) and the power radiated (dotted line)

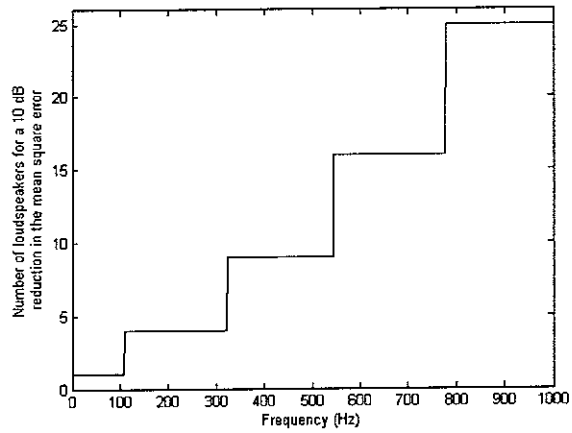

Figure 4.4. Number of loudspeakers required for a 10 dB reduction in the mean-square excitation error

The results for the sound reduction index calculated using both the free field diffuse model, described above, and calculated using the pressure field generated with four near field loudspeakers are presented in Figure 4.5. In the low frequency range the sound reduction index calculated using the array of loudspeakers is very similar to that calculated using the true diffuse field. As the frequency increases, the differences between the sound reduction index calculated using the two different methods get larger, but errors of less than 5 dB are incurred up to 500 Hz even for this very lightly damped panel ($\zeta = 1\%$).

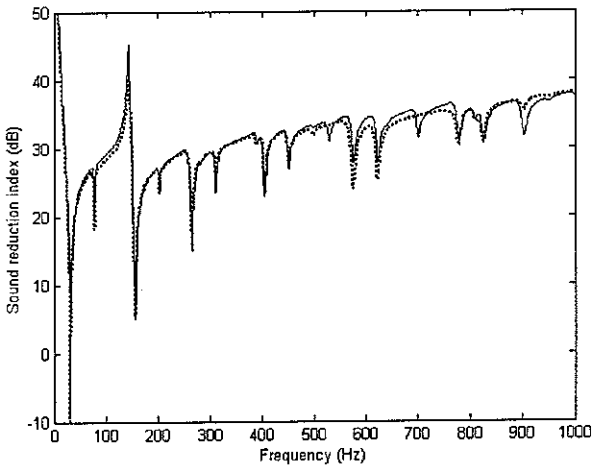

Figure 4.5. Sound reduction index calculated for a diffuse field excitation under free radiation conditions (solid line), and calculated from the pressure field generated by four near field loudspeakers with optimised signals, also under free field conditions (dotted line)

It has to be noted that the overall level for the sound reduction index in this figure is different from the one calculated in Section 3.3, where the diffuse sound field has been considered as a superposition of propagating waves from uniformly distributed directions in the space. This dissimilarity appears due to the different expressions used for the calculation of the incident power on the panel. Figure 4.6 illustrates these effects with the calculation of the sound reduction index for the aluminium partition

using Eq. (4.10) with the theoretical expression for the spectral density matrix (Eq. 4.9), using the same equation for each of the incident plane waves arriving on the panel, and integrating the contribution of each plane wave over the whole semispace, Eq. (3.29). The differences between the two first graphs are due to the limited number of incident plane waves for the simulation of the diffuse field. The differences with the third graphs arise because the different expression for the calculation of the incident power.

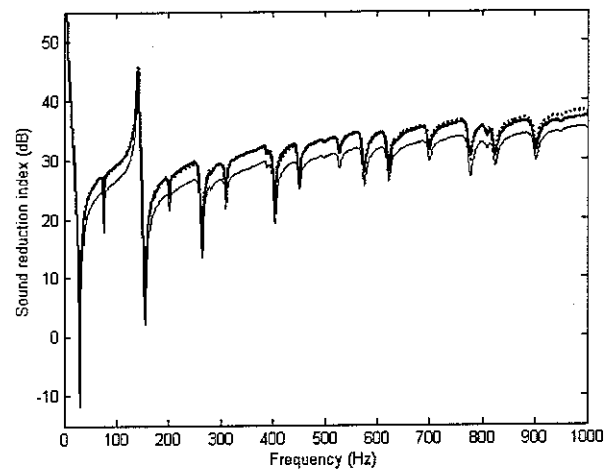

Figure 4.6. Sound reduction index calculated for a diffuse field excitation under free radiation conditions using Eq. (4.10) and the theoretical expression for S_{dd} (bold), using Eq. (4.10) for a diffuse field due to a number of plane waves (dotted), and integrating the contribution of each plane wave over the whole semi-space, Eq. (3.29) (solid)

4.1.3 Comparison with an array of uncorrelated loudspeakers

The good behaviour observed for the sound reduction index over the frequency range would not be expected from the error in the panel response calculated in Figure 4.3. To find out more about the nature of the reproduction for the excitation and the response, the same set of simulations have been repeated with an array of uncorrelated loudspeakers.

Two different cases have been considered. In the first one, the array is driven by four independent reference signals and the loudspeakers are totally uncorrelated. The matrix of filters $\mathbf{W}$ has all zero entries excepting the first diagonal. In the second case, the array is driven by the same reference signal and the loudspeakers are totally correlated. The matrix of filters $\mathbf{W}$ has all zero entries excepting the first column. The results for the two cases are presented in Figure 4.7 (a) and (b), respectively.

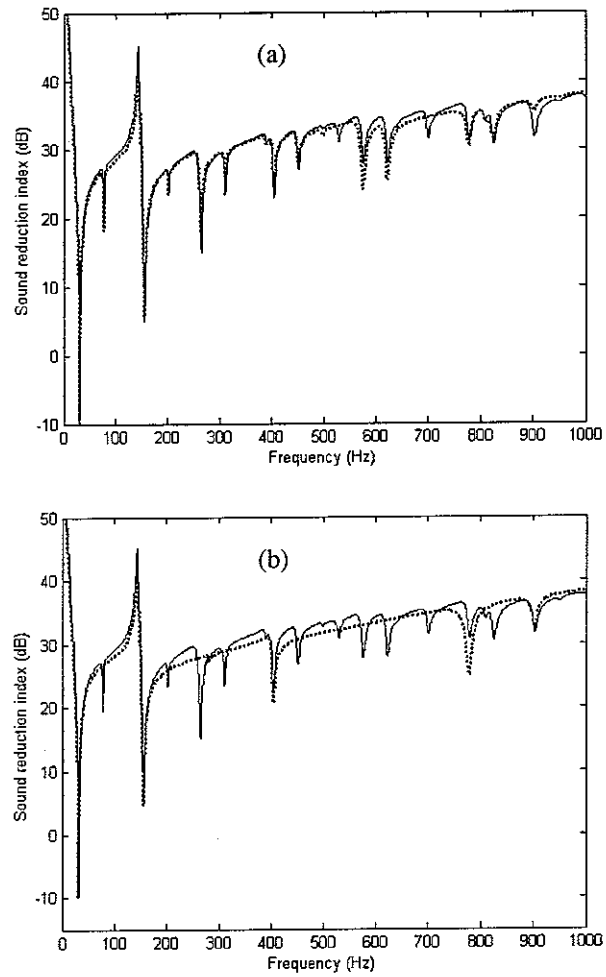

Figure 4.7. Sound reduction index for a four-loudspeakers array: theoretical (solid line) and obtained with the loudspeakers (dotted line) when these are uncorrelated (a) and correlated (b)

As it can observe, the results obtained with the four uncorrelated loudspeakers are very similar to the optimised ones. To make a more detailed comparison for the two cases, the spatial correlation function between the central row of microphones over the panel (Figure 4.8) has been studied.

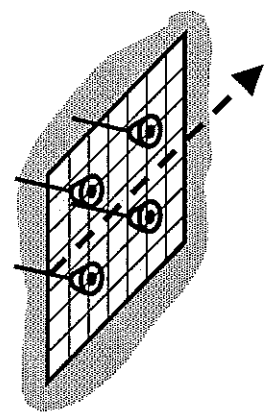

Figure 4.8. Central row of microphones over the panel to calculate the spatial correlation function

The results for the excitation with the optimised array, the uncorrelated loudspeakers and the theoretical diffuse field are compared at 100 and 600 Hz in Figure 4.9.

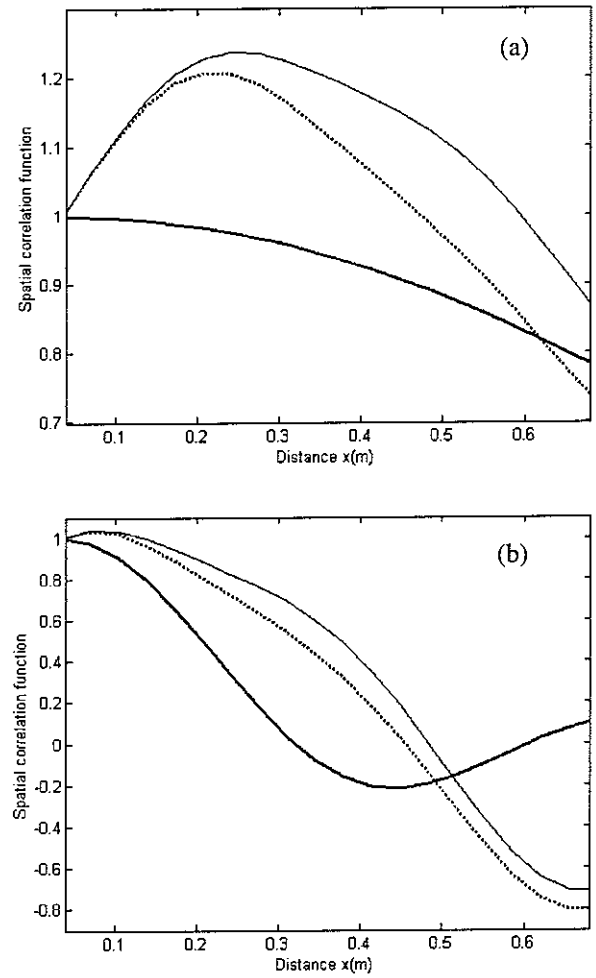

Figure 4.9. Spatial correlation function for the excitation over the panel (microphones over the centre) in free field obtained with four loudspeakers: theoretical (solid), with optimised loudspeakers (dash-dotted) and with uncorrelated loudspeakers (dashed) at 100 Hz (a) and 600 Hz (b)

As it can be expected, the results obtained for the reproduction of the excitation with a fixed number of loudspeakers become worse as the frequency is increased. It can also be observed that the figures for the optimised and uncorrelated array are very similar. Although the results are not presented here, the figures for the velocity and power radiated spectra show similar trends when comparing the optimised and uncorrelated array.

The comparison is completed with the results for the incident and the radiated power, as shown in Figure 4.10. The optimised array is not able to provide the required incident power in the high frequency range, and the radiated power is also below. The sound reduction index for the two cases, presented previously in Figures 4.5 and 4.7 (a), are compared together in Figure 4.11. As it has been pointed out before, both figures are almost identical.

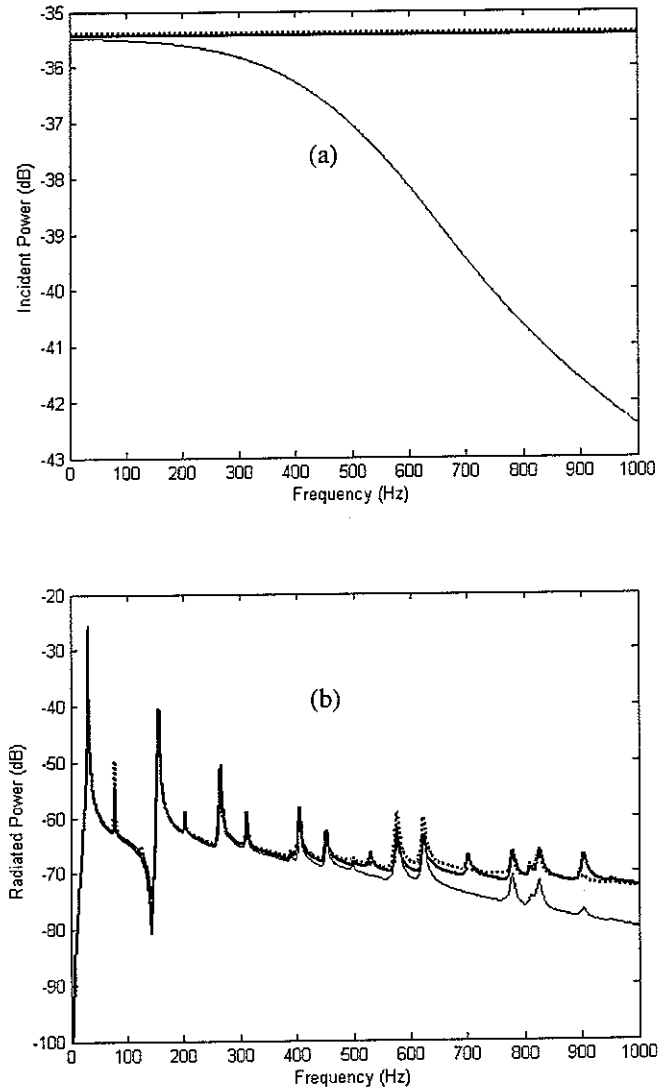

Figure 4.10. Incident power (a) and radiated power (b) in free field obtained with four loudspeakers: theoretical (bold), with optimised loudspeakers (solid) and with uncorrelated loudspeakers (dotted)

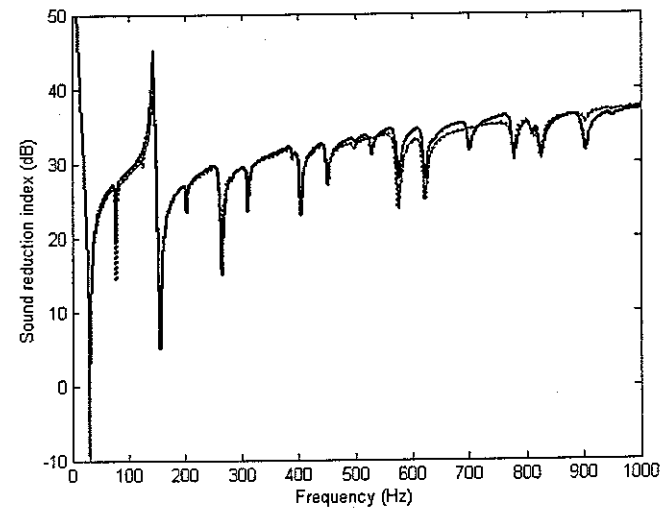

Figure 4.11. Sound reduction index in free field obtained with four loudspeakers: theoretical (bold), with optimised loudspeakers (solid) and with uncorrelated loudspeakers (dotted)

To observe differences between the optimised and the uncorrelated set of loudspeakers it is necessary to use an array of three by three actuators. The corresponding sound reduction indexes are represented in Figure 4.12. In this case, the optimised array of loudspeakers is able to reproduce the theoretical one over the whole frequency range. The discrepancies with the uncorrelated array appear mainly in the (2, 2) panel mode, with a corresponding natural frequency of 125 Hz, showing differences of around 8 dB.

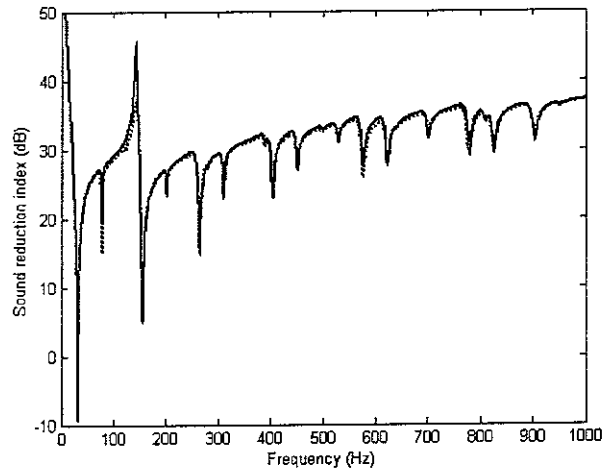

Figure 4.12. Sound reduction index in free field obtained with nine loudspeakers: theoretical (bold), with optimised loudspeakers (solid) and with uncorrelated loudspeakers (dotted)

The same procedure has been used to study the influence of the partition size, damping and type of materials. The results obtained are showing the same behaviour that the aluminium panel analysed before in detail. The results in Figure 4.12 are represented again in Figure 4.13 for a (2.5 x 2.5 x 0.003) m aluminium panel. Although four loudspeakers are not able to provide the same good results than before in the high frequency range, the behaviour of the optimised and uncorrelated loudspeakers shows the same general trend.

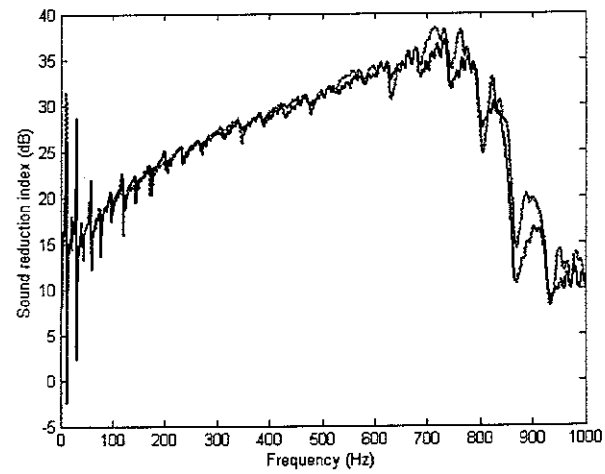

Figure 4.13. Sound reduction index in free field obtained with four loudspeakers for a (2.5 x 2.5 x 0.003) m aluminium panel: theoretical (bold), with optimised loudspeakers (solid) and with uncorrelated loudspeakers (dotted)

4.2 Aluminium partition coupled to the source room only

4.2.1 Analytical expressions

In this section, the reproduction of a diffuse pressure field when the aluminium partition is coupled to the source room only and radiates to free field will be analysed.

To characterise the incident sound power in the source room, the mean square sound pressure averaged in a number of positions through the cavity should be determined. Previously, we have related this quantity to the acoustical potential energy in the room and expressed the sound reduction index as a function of the amplitudes of the normal modes for the fully coupled system. As the objective now is to simulate a diffuse field with an optimised array of loudspeakers only over the panel surface, to calculate the sound reduction index we will consider the mean square sound pressure average on the positions of the array of microphones over the panel, as:

$$\Pi_{\text{inc}} = \frac{s_r \operatorname{Tr}(\mathbf{y}\mathbf{y}^{\text{H}})}{4\rho_0 c_0} = \frac{s_r \operatorname{Tr}(\mathbf{G}\mathbf{W}_{\text{opt}}\mathbf{W}_{\text{opt}}^{\text{H}}\mathbf{G}^{\text{H}})}{4\rho_0 c_0}, \tag{4.17}$$

where s_r is the surface of the elements in the grid of microphones, that is the same than the elemental radiators for this case, and $\mathbf{G}$ is the transfer function between the loudspeakers and the microphone positions for a cavity-panel coupled system, that has been studied in Section 2.2. Substituting the value for $\mathbf{W}_{\text{opt}}$, given by Eq. (4.2):

$$\Pi_{\text{inc opt}} = \frac{s_r \operatorname{Tr}(\mathbf{G}\mathbf{G}^{\dagger}\mathbf{S}_{dd}\mathbf{G}^{\dagger^{\text{H}}}\mathbf{G}^{\text{H}})}{4\rho_0 c_0}. \tag{4.18}$$

If the loudspeakers are uncorrelated, the corresponding incident power over the array of microphones is given by

$$\Pi_{\text{inc}} = \frac{s_r \operatorname{Tr}(\mathbf{G}\mathbf{W}\mathbf{W}^{\text{H}}\mathbf{G}^{\text{H}})}{4\rho_0 c_0} \tag{4.19}$$

where $\mathbf{W}$ is the matrix of source strengths, whose first diagonal elements are equal to unity when the signals are not optimised, and the other elements are zero.

For completeness and comparison with the classical measurement procedure, the incident sound power over the panel calculated using the average sound pressure level in the source room takes the expression:

$$\Pi_{\text{inc ep}} = \frac{S_p \operatorname{Tr}(\mathbf{a}_1^{(\text{I})}\mathbf{G}^{\dagger}\mathbf{S}_{dd}\mathbf{G}^{\dagger^{\text{H}}}\mathbf{a}_1^{(\text{I})^{\text{H}}})}{4\rho_0 c_0} \tag{4.20}$$

where $\mathbf{a}_1^{(\text{I})}$ are the normal modes amplitudes for the source room, Eq. (2.13).

The radiated power has been calculated with the same expression than for the panel in an infinite baffle, Eq. (4.6). It reads:

$$\Pi_{\text{trans}} = \mathbf{a}^{(p)\text{H}}\mathbf{M}\mathbf{a}^{(p)} = \mathbf{a}^{(p)\text{H}}\boldsymbol{\varphi}^{\text{H}}\mathbf{R}\boldsymbol{\varphi}\mathbf{a}^{(p)}, \tag{4.21}$$

but the modal panel amplitudes, $\mathbf{a}^{(p)}$, have been obtained from the coupled cavity-panel system as:

$$\mathbf{a}^{(p)} = \mathbf{A}_p\mathbf{G}^{(1)}\mathbf{a}^{(1)} = \mathbf{G}_p^{(1)}\mathbf{a}^{(1)}. \tag{4.22}$$

The final expression for the transmitted power when the loudspeaker array is optimised is given by:

$$\Pi_{\text{trans opt}} = \text{Tr}\left(\mathbf{S}_{dd}\mathbf{G}^{\dagger\text{H}}\mathbf{a}^{(1)\text{H}}\mathbf{G}_p^{(1)\text{H}}\boldsymbol{\varphi}^{\text{H}}\mathbf{R}\boldsymbol{\varphi}\mathbf{G}_p^{(1)}\mathbf{a}^{(1)}\mathbf{G}^{\dagger}\right), \tag{4.23}$$

When the loudspeakers are not optimised, it reads:

$$\Pi_{\text{trans}} = \text{Tr}\left(\mathbf{W}\mathbf{W}^{\text{H}}\mathbf{a}^{(1)\text{H}}\mathbf{G}_p^{(1)\text{H}}\boldsymbol{\varphi}^{\text{H}}\mathbf{R}\boldsymbol{\varphi}\mathbf{G}_p^{(1)}\mathbf{a}^{(1)}\right). \tag{4.24}$$

4.2.2 Numerical simulations

The equations derived in the previous sections have been implemented in a Matlab program to reproduce the sound reduction for the cavity-panel coupled system. An array of 20 x 20 uniformly spaced microphones situated over the panel has been exposed to the pressure field generated by an array of 2 x 2 loudspeakers, whose inputs are calculated according to Eq. (4.2). A schematic representation of the system is shown in Figure 4.14.

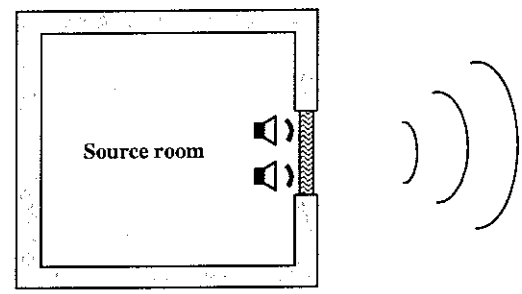

Figure 4.14. Four-loudspeaker array acting over the panel coupled to the source room

The spatial correlation function for the optimised and uncorrelated set of loudspeakers, has been calculated again between the central row of microphones over the panel. The results for the excitation are represented in Figure 4.15 for 100 Hz and 600 Hz. When comparing this figure with the results from Figure 4.8, obtained for the panel in an infinite baffle radiating to free field, it can be appreciated that the reproduction is slightly worse for 100 Hz in the case of the cavity-panel system, and very similar to the free field case for 600 Hz.

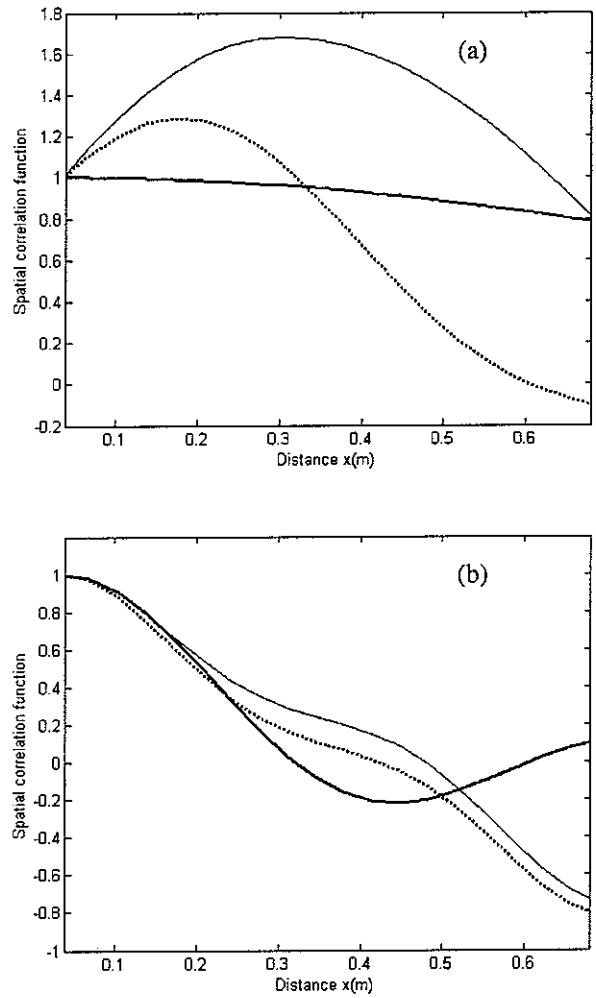

Figure 4.15. Spatial correlation function for the excitation over the panel (microphones over the centre) in the cavity-panel configuration obtained with four loudspeakers: theoretical (solid), with optimised loudspeakers (dash-dotted) and with uncorrelated loudspeakers (dashed) at 100 Hz (a) and 600 Hz (b)

The incident and radiated power (Eqs. 4.17 and 4.23) are represented in Figure 4.16. In this case the frequency axis has been represented up to 600 Hz due to convergence limitations. The results for the incident power and the optimised loudspeaker array are similar to those obtained in free field. The loudspeaker array provides a good approximation to the free field incident power, although the level decreases as we increase the frequency range. On the other hand, the results for the uncorrelated loudspeakers are completely different, as they show the modal behaviour of the source room over the microphone positions. The same trend can be appreciated from the result for the radiated sound power (Figure 4.16 (b)). The four optimised actuators are able to reproduce the theoretical results reasonably well, although some of the room normal modes are visible. For the uncorrelated loudspeakers the graph does not follow the true diffuse one, showing the source room behaviour clearly.

For a comparison with the classical method, the incident power over the aluminium partition using the average sound pressure level in the source room has been calculated using Eq. (4.20) for the optimised and uncorrelated array of loudspeakers. The results are presented in Figure 4.17.

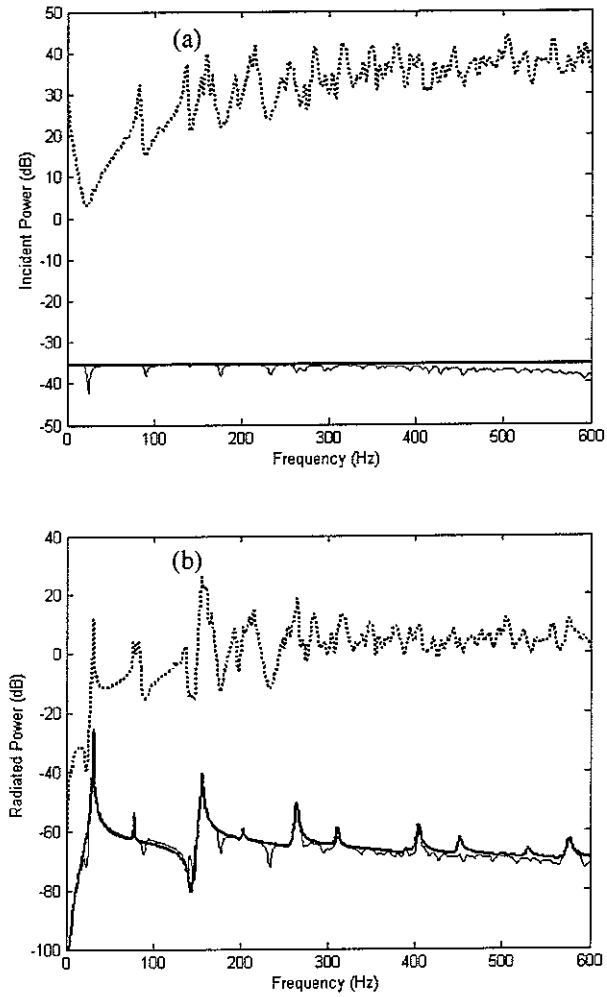

Figure 4.16. Incident power (a) and radiated power (b) in the cavity-panel configuration obtained with four loudspeakers: theoretical (bold), with optimised loudspeakers (solid) and with uncorrelated loudspeakers (dotted)

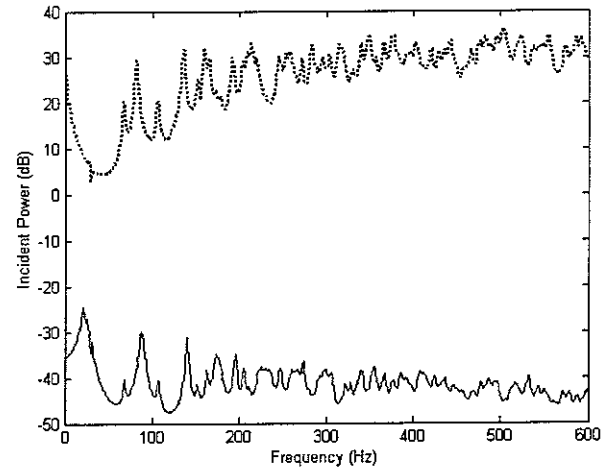

Figure 4.17. Incident power in the cavity-panel configuration calculated with the average sound pressure level in the source room for a four-loudspeakers array: optimised loudspeakers (solid) and uncorrelated loudspeakers (dotted)

The ratio of the incident and radiated power is shown in Figure 4.18. In the very low frequency range, below 50 Hz, both optimised and uncorrelated loudspeakers provide the same results, showing good agreement with the theoretical ones. Between 50 Hz and 300 Hz the effect of the optimisation is more clearly seen, with differences with respect to the uncorrelated array up to 5 dB. Above 300 Hz the optimised array is not able to provide good results, and the behaviour of the two set of loudspeakers is similar.

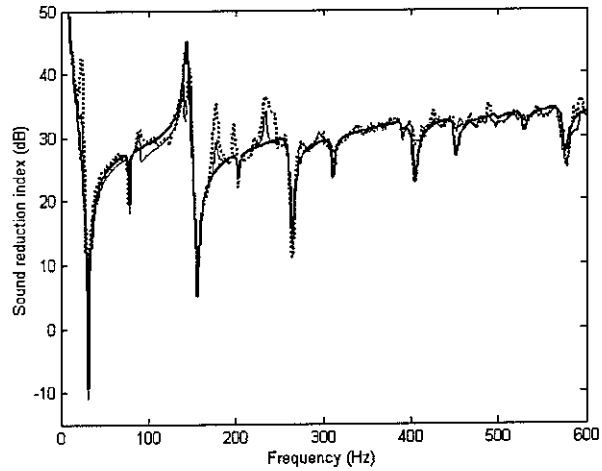

Figure 4.18. Sound reduction index in the cavity-panel configuration obtained with four loudspeakers: theoretical (bold), with optimised loudspeakers (solid) and with uncorrelated loudspeakers (dotted)

To obtain a better approximation over the whole frequency range it is necessary to consider an array of 4 x 4 loudspeakers. The sound reduction index for sixteen loudspeakers is presented in Figure 4.19, in which the optimised array provides a result almost identical to the theoretical one. The differences with the uncorrelated set are the same than when using four loudspeakers.

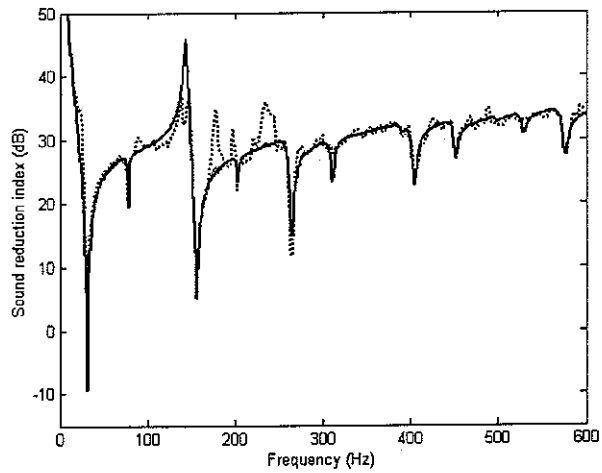

Figure 4.19. Sound reduction index in the cavity-panel configuration obtained with sixteen loudspeakers: theoretical (bold), with optimised loudspeakers (solid) and with uncorrelated loudspeakers (dotted)

To summarise the results obtained in this section, a comparison between the classical method for the determination of the sound reduction index and the near field loudspeaker array is presented in the next figures. Four far-field loudspeakers have been distributed over the source room, driven by

uncorrelated reference signals. The incident power, calculated as the average sound pressure level over the whole cavity, Eq. (3.3), is compared with the near field results in Figure 4.20 (a). The corresponding sound power radiated is also shown (b).

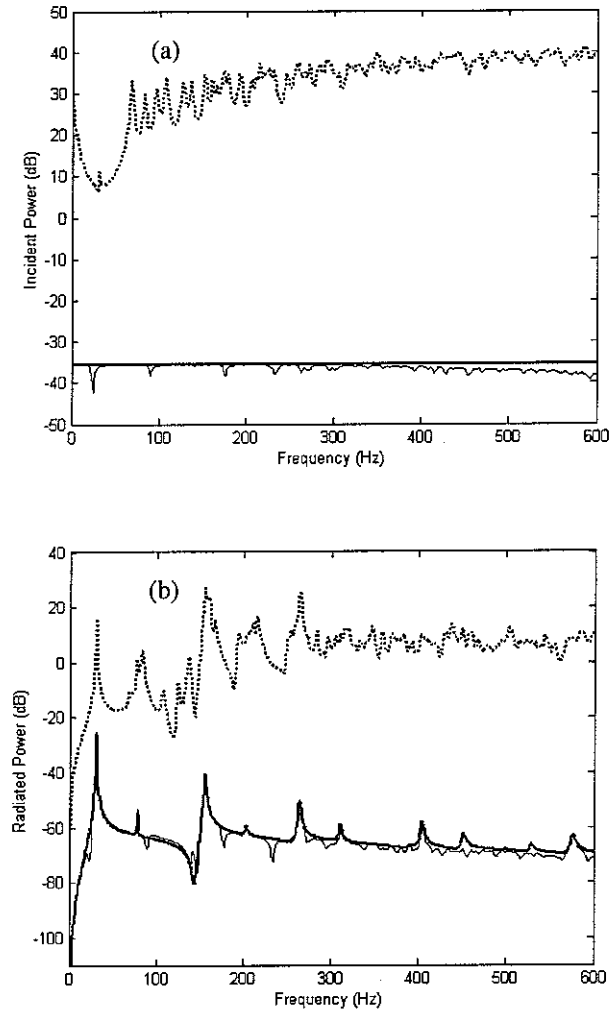

Figure 4.20. Incident power (a) and radiated power (b) in the cavity-panel configuration obtained with four loudspeakers: theoretical (bold), near-field optimised loudspeakers (solid) and far-field uncorrelated loudspeakers (dotted)

The sound reduction index obtained with the four far field loudspeakers and the classical formulation is compared in Figure 4.21 with the near field array. Even with this number of loudspeakers, the improvement removing the modal behaviour of the source room, especially below 300 Hz, is clear.

Finally, the dimensions of the source room have been increases up to (3.07 x 3.52 x 3.51) m, and the classical and near field methods have been applied in the calculation of the sound reduction index, as shown in Figure 4.22. As it would be expected, the results for the classical methods have varied considerably as they depend closely in the modal room behaviour. The performance of the four near field loudspeakers is very similar, following closely the pure diffuse sound reduction index.

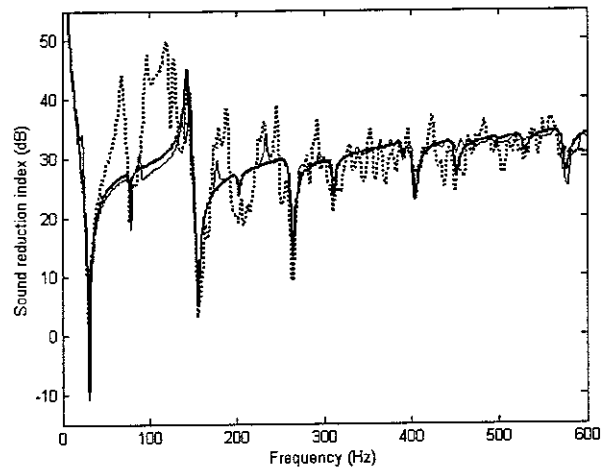

Figure 4.21. Sound reduction index in the cavity-panel configuration obtained with four loudspeakers: theoretical (bold), near-field optimised loudspeakers (solid) and far-field uncorrelated loudspeakers (dotted)

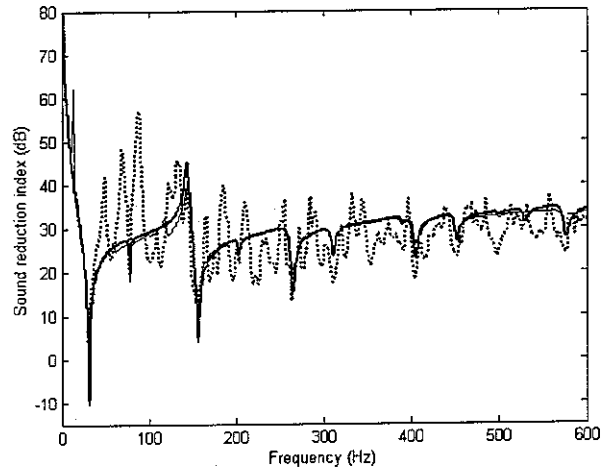

Figure 4.22. Sound reduction index in the cavity-panel configuration for a (3.07 x 3.52 x 3.51) m source room obtained with four loudspeakers: theoretical (bold), near-field optimised loudspeakers (solid) and far-field uncorrelated loudspeakers (dotted)

4.3 Aluminium partition in the transmission suite

4.3.1 Analytical expressions

When the aluminium partition is suited in the transmission suite, the expression for the incident power over the panel is the same than Eq. (4.17):

$$\Pi_{\text{inc opt}} = \frac{s_r \,\text{Tr}(\mathbf{G}\mathbf{G}^{\dagger}\mathbf{S}_{dd}\mathbf{G}^{\dagger^{\text{H}}}\mathbf{G}^{\text{H}})}{4\rho_0 c_0}, \tag{4.25}$$

but in this case it is necessary to change the matrix of transfer functions between loudspeakers and microphones, $\mathbf{G}$, to take into account also the coupling of the panel with the receiving room, as analysed in Section 2.3.2. for a fully-coupled system.

When the loudspeakers are not optimised, the corresponding incident power over the array of microphones is given by Eq. (4.18)

$$\Pi_{\text{inc}} = \frac{s_r \,\text{Tr}(\mathbf{G}\mathbf{W}\mathbf{W}^{\text{H}}\mathbf{G}^{\text{H}})}{4\rho_0 c_0}. \tag{4.26}$$

For the radiated power, we could use the expression for the potential energy in the receiving room or the mean-square sound pressure, averaged on the positions of the elemental radiators over the panel. In the first case, the normal modes amplitudes in a fully-coupled system for the second cavity, $\mathbf{a}^{(2)}$, as a function of the normal modes amplitudes for the source room, $\mathbf{a}^{(1)}$, have been previously calculated as:

$$\mathbf{a}^{(2)} = -(\mathbf{Z}_2)^{-1}\mathbf{Z}_a^{(2)}\mathbf{a}^{(1)}, \tag{4.27}$$

where the matrices $\mathbf{Z}_2$ and $\mathbf{Z}_a^{(2)}$ have been defined in Eqs. (2.50) and (2.51) respectively. When the loudspeaker array is optimised to reproduce the diffuse sound field,

$$\mathbf{a}^{(2)} = -(\mathbf{Z}_2)^{-1}\mathbf{Z}_a^{(2)}\mathbf{a}^{(1)}\mathbf{G}^{\dagger}\mathbf{D} = \mathbf{Z}_{12}\mathbf{a}^{(1)}\mathbf{G}^{\dagger}\mathbf{D}, \tag{4.28}$$

and the radiated power using the average sound pressure level over the receiving room can be expressed as:

$$\Pi_{\text{trans}\,ep} = \frac{A_{\text{rec}} Tr(\mathbf{a}^{(2)}\mathbf{a}^{(2)^{\text{H}}})}{4\rho_0 c_0} = \frac{A_{\text{rec}} Tr(\mathbf{Z}_{12}\mathbf{a}^{(1)}\mathbf{G}^{\dagger}\mathbf{S}_{dd}\mathbf{G}^{\dagger^{\text{H}}}\mathbf{a}^{(1)^{\text{H}}}\mathbf{Z}_{12}{}^{\text{H}})}{4\rho_0 c_0}. \tag{4.29}$$

When the loudspeaker array is not optimised, the radiated power is given by:

$$\Pi_{\text{trans}} = \frac{A_{\text{rec}}\,\text{Tr}(\mathbf{Z}_{12}\mathbf{a}^{(1)}\mathbf{W}\mathbf{W}^{\text{H}}\mathbf{a}^{(1)^{\text{H}}}\mathbf{Z}_{12}{}^{\text{H}})}{4\rho_0 c_0}. \tag{4.30}$$

Instead of using the potential energy in the receiving room, we could use the mean square sound pressure averaged on the positions of the elemental radiators over the panel. In this case, the acoustic power radiated by this array of elemental sources is proportional to the real part of the sum of the conjugate volume velocities of each radiator, $\mathbf{v}$, multiplied by the corresponding acoustic pressure in the receiving room, $\mathbf{p}^{(2)}$ immediately in front of each source

$$\Pi_{\text{trans}} = \frac{s_r}{2}\text{Re}\left[\mathbf{v}^{\text{H}}\mathbf{p}^{(2)}\right], \tag{4.31}$$

where s_r is the surface of the elementary radiators, assumed to be of equal size. The pressure for the second cavity in the positions of the elemental radiators when the loudspeaker array is optimised to reproduce the diffuse field is given by:

$$\mathbf{p}^{(2)} = \mathbf{\Psi}\mathbf{a}^{(2)} = \mathbf{\Psi}\mathbf{Z}_{12}\mathbf{a}^{(1)}\mathbf{G}^{\dagger}\mathbf{D}, \tag{4.32}$$

where $\mathbf{\Psi}$ is the matrix of normal cavity modes evaluated at the positions of the elementary radiators.

The vector of complex linear velocities at the positions of the elemental radiators can be written as:

$$\mathbf{v} = \boldsymbol{\varphi}\mathbf{a}_p, \tag{4.33}$$

in which the elements of the matrix φ are the normal panel modes evaluated at the positions of the elementary radiators. The expression for the radiated power then takes the form:

$$\Pi_{\text{trans opt}} = \frac{S_r}{2}\text{Re}\left[\mathbf{a}_p^{\text{H}}\boldsymbol{\varphi}^{\text{H}}\boldsymbol{\Psi}\mathbf{Z}_{12}\mathbf{a}^{(1)}\mathbf{G}^{\dagger}\mathbf{D}\right]. \tag{4.34}$$

The complex panel modal amplitudes for the fully coupled system has been calculated in Section 2.3.2. as:

$$\mathbf{a}_p = \mathbf{A}_p(\mathbf{G}^{(1)}\mathbf{a}^{(1)} - \mathbf{G}^{(2)}\mathbf{a}^{(2)}), \tag{4.35}$$

where $\mathbf{A}_p$ is the matrix of modal resonance terms, and $\mathbf{G}^{(1)}$ and $\mathbf{G}^{(2)}$ are the modal coupling coefficient matrices between the panel and the source and receiving room, respectively. When the loudspeaker array is optimised, the modal panel amplitudes are given by:

$$\mathbf{a}_p = \mathbf{A}_p(\mathbf{G}^{(1)}\mathbf{a}^{(1)}\mathbf{G}^{\dagger}\mathbf{D} - \mathbf{G}^{(2)}\mathbf{Z}_{12}\mathbf{a}^{(1)}\mathbf{G}^{\dagger}\mathbf{D}). \tag{4.36}$$

Operating and taking $\mathbf{G}_p^{(1)} = \mathbf{A}_p\mathbf{G}^{(1)}$, we obtain

$$\mathbf{a}_p = (\mathbf{G}_p^{(1)} - \mathbf{G}_p^{(2)}\mathbf{Z}_{12})\mathbf{a}^{(1)}\mathbf{G}^{\dagger}\mathbf{D}. \tag{4.37}$$

Substituting the value for $\mathbf{a}_p$ in the expression for the radiated power, Eq. (4.34), it follows:

$$\Pi_{\text{trans opt}} = \frac{S_r}{2}Tr\left(\text{Re}\left[\mathbf{S}_{dd}\mathbf{G}^{\dagger\text{H}}\mathbf{a}^{(1)\text{H}}(\mathbf{G}_p^{(1)\text{H}} - \mathbf{Z}_{12}{}^{\text{H}}\mathbf{G}_p^{(2)\text{H}})\boldsymbol{\varphi}^{\text{H}}\boldsymbol{\Psi}\mathbf{Z}_{12}\mathbf{a}^{(1)}\mathbf{G}^{\dagger}\right]\right). \tag{4.38}$$

In the case when the loudspeaker array is not optimised, the expression for the transmitted power takes the form:

$$\Pi_{\text{trans}} = \frac{S_r}{2}Tr\left(\text{Re}\left[\mathbf{W}^{\text{H}}\mathbf{a}^{(1)\text{H}}(\mathbf{G}_p^{(1)\text{H}} - \mathbf{Z}_{12}{}^{\text{H}}\mathbf{G}_p^{(2)\text{H}})\boldsymbol{\varphi}^{\text{H}}\boldsymbol{\Psi}\mathbf{Z}_{12}\mathbf{a}^{(1)}\mathbf{W}\right]\right). \tag{4.39}$$

4.3.2 Numerical simulations

The previous equations have been implemented again in a Matlab program to reproduce the sound reduction index for the cavity-panel-cavity fully-coupled system. An array of 20 x 20 uniformly spaced microphones situated over the panel has been exposed to the pressure field generated by an array of 2 x 2 loudspeakers, whose outputs are calculated according to Eq. (4.2). Although to obtain a better excitation reproduction it would be desirable to increase the number of loudspeakers in the array, to make a direct comparison with the cases analysed previously the same four near field

loudspeakers array has been employed in the numerical simulations. A simplified representation of the system is shown in Figure 4.23.

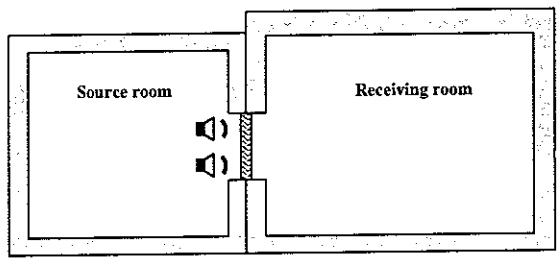

Figure 4.23. Four-loudspeakers array acting over the panel in the transmission suite

The spatial correlation function for the four optimised and uncorrelated set of loudspeakers, has been calculated again between the central row of microphones over the panel (Figure 4.6). The results for the excitation are shown in Figure 4.24 for 100 Hz and 600 Hz. Comparing this result with the cavity-panel system, Figure 4.14, no fundamental differences can be appreciated.

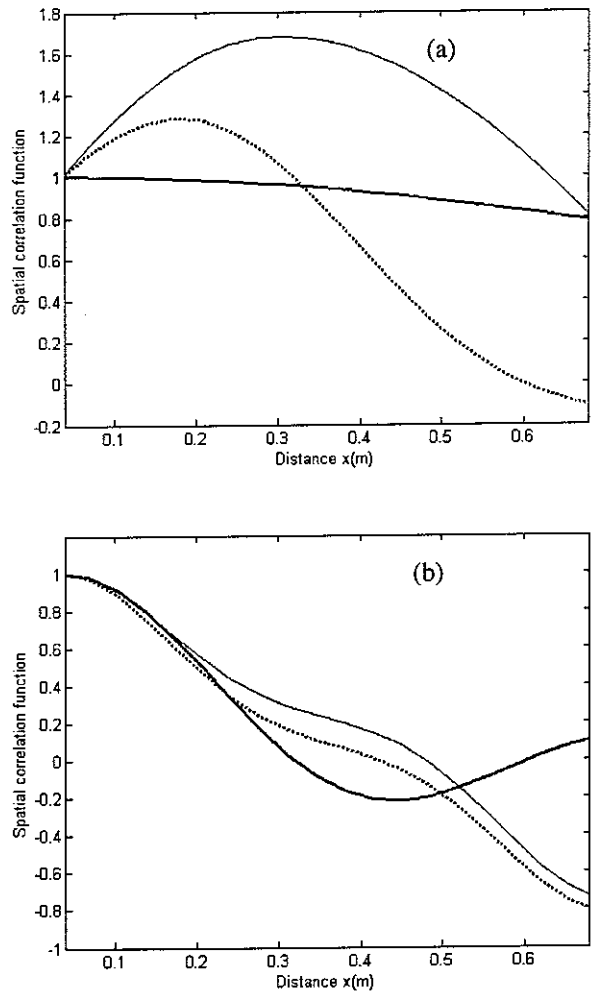

Figure 4.24. Spatial correlation function for the excitation over the panel (microphones over the centre) in the transmission suite obtained with four loudspeakers: theoretical (solid), with optimised loudspeakers (dash-dotted) and with uncorrelated loudspeakers (dashed) at 100 Hz (a) and 600 Hz (b)

The results for the incident and radiated power are represented in Figure 4.25. The incident and radiated power have been calculated using the intensity in the source and receiving rooms, Eqs. (4.25) and (4.38). Although the incident power is reasonably well reproduce with the four loudspeakers array, the presence of the receiving room makes the reproduction of the radiated power very poor in comparison with the panel-cavity system (Figure 4.16 (b)).

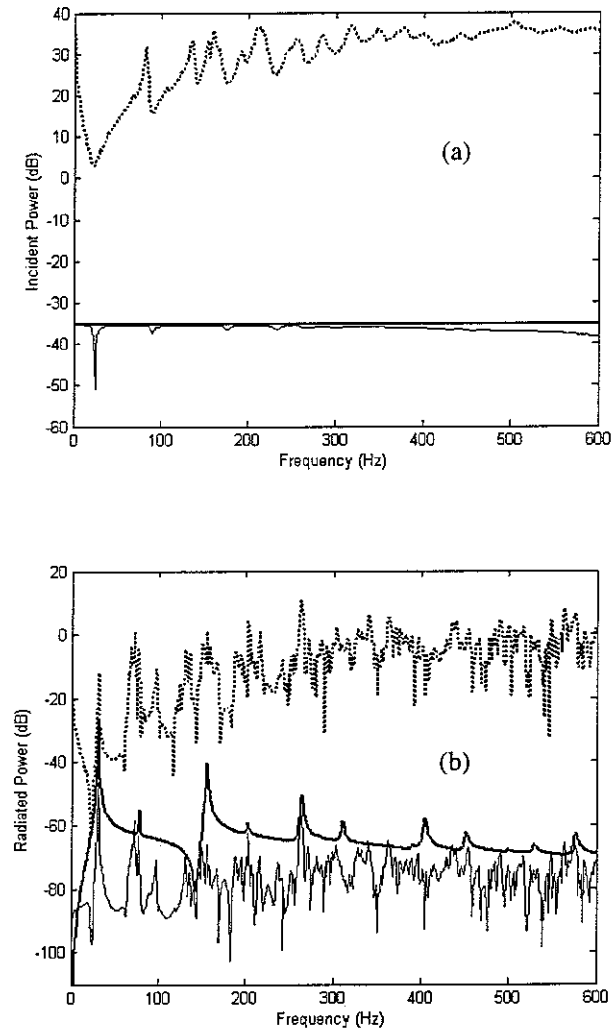

Figure 4.25. Incident power (a) and radiated power (b) in the transmission suite obtained with four loudspeakers: theoretical (bold), with optimised loudspeakers (solid) and with uncorrelated loudspeakers (dotted)

For a comparison with the classical method, the incident and radiated power using the average sound pressure level in the source and receiving rooms have been calculated using Eqs. (4.20) and (4.29) for the optimised and uncorrelated array of loudspeakers. The results are presented in Figure 4.26. For the incident power, the two results are almost the same than for the cavity-panel configuration because the coupling with the second cavity is very weak. For the radiated power, the optimisation in the source room is unnoticeable in the receiving enclosure.

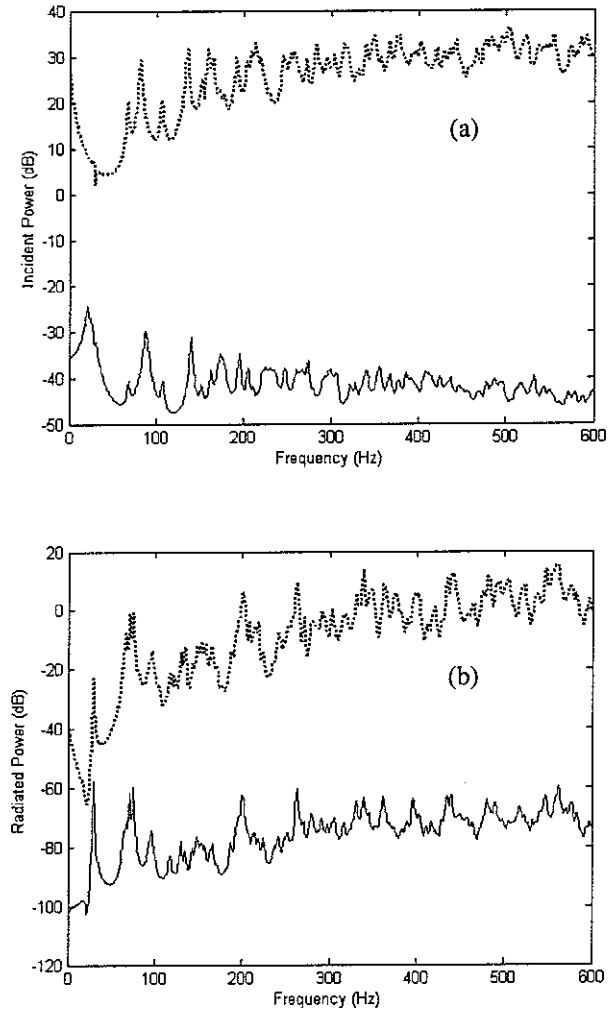

Figure 4.26. Incident power (a) and radiated power (b) in the transmission suite calculated with the average sound pressure level in the source room and the receiving room for a four-loudspeakers array: optimised loudspeakers (solid) and uncorrelated loudspeakers (dotted)

The results for the sound reduction index using the intensity expressions are shown in Figure 4.27. As it can be seen, the reproduction of the excitation in the source room does not produce any noticeable improvement in the sound reduction index between the optimised and the uncorrelated set of loudspeakers. These results do not improved with an increasing number of near-field loudspeakers.

For the calculation of the sound reduction index using the intensity method, ideally, the receiving space should be very quiet and non reverberant as in the case of an anechoic room (Croker *et* al., 1981). In practice, almost any relatively non-reverberant environment on the receiving side of the panel is sufficient, provided the background noise levels are low. In an attempt to reproduce this real situation, the damping term for the receiving room has been increased from 8% to 30%. The final results obtained for the sound reduction index are presented in Figure 4.28. As it can be observed, some differences appear when comparing with Figure 4.27, but the results obtained are still far away from the free field ones.

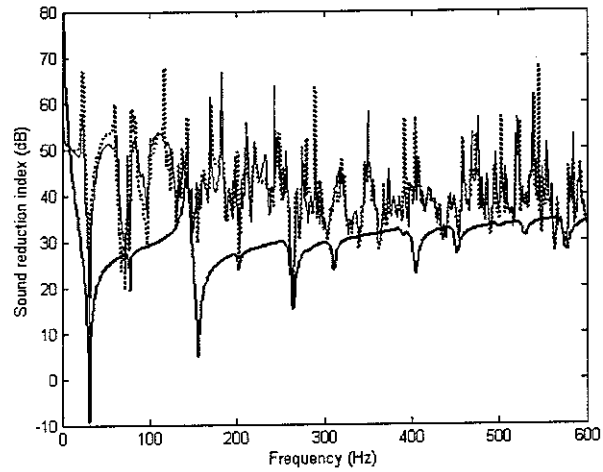

Figure 4.27. Sound reduction index in the transmission suite obtained with four loudspeakers: theoretical (bold), with optimised loudspeakers (solid) and with uncorrelated loudspeakers (dotted)

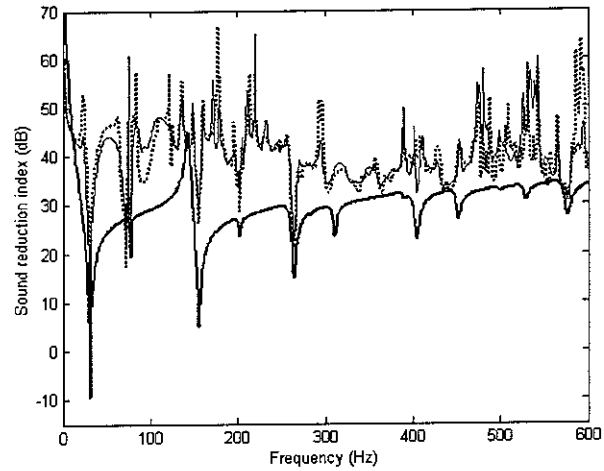

Figure 4.28. Sound reduction index in the cavity-panel configuration obtained with sixteen loudspeakers and $\overline{\alpha}$ = 30% in the receiving room: theoretical (bold), with optimised loudspeakers (solid) and with uncorrelated loudspeakers (dotted)

To finish with this section, the results for the sound reduction index using four uncorrelated far field loudspeakers and the classical formulation are shown in Figure 4.29. The results for the sound reduction index in the low frequency range are similar for the near field and far field results. Above 300 Hz the optimised results follows more closely the general variation of the pure diffuse ones.

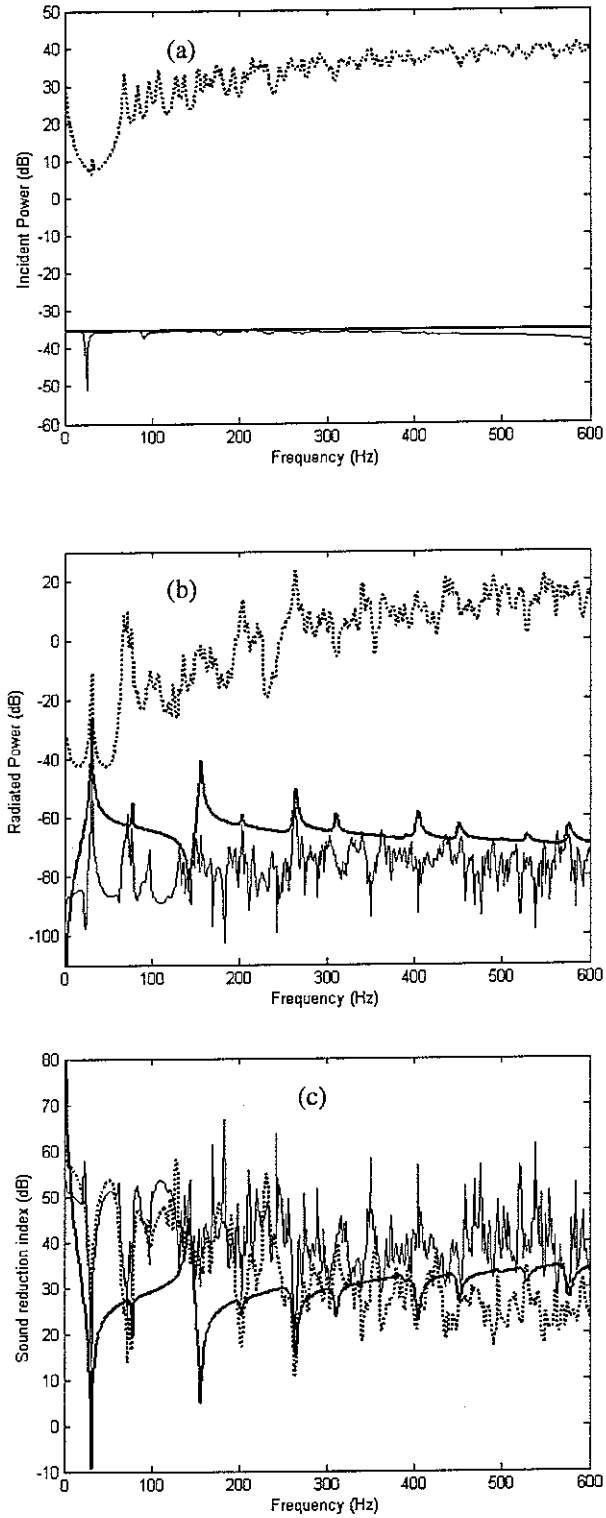

Figure 4.29. Incident power (a), radiated power (b) and sound reduction index (c) in the transmission suite obtained with four loudspeakers: theoretical (bold), near-field optimised loudspeakers (solid) and far-field uncorrelated loudspeakers (dotted)

5. SUMMARY AND CONCLUSIONS

This report has discussed the determination of the sound reduction index of flexible partitions. The measurements from different transmission suites, where an acoustic field is generated by loudspeakers, and transmitted from the source to the receiving room must be treated with caution. In the low frequency range, the sound field in the rooms is dominated by very few normal modes, and the facilities do not satisfy diffuse field conditions. The use of different geometries can lead to a wide spread of results.

Although this problem is not new, no solution has been proposed to deal with the nature of the pressure field itself. In this work, a new approach based in the generation of a pressure distribution with the same spatial correlation characteristics than a diffuse field has been proposed, using an array of near field loudspeakers and microphones.

Before studying the feasibility of the diffuse field reproduction, an analytical formulation to determined the sound reduction index has been applied and compared in three different situations: two rooms coupled by a partition, the source room coupled to the panel and radiating to free field, and the panel in an infinite baffle radiating to free field. The determination of the sound reduction index has been formulated using a modal approach for the cavities and the panel. The results obtained in the numerical simulations show discrepancies than more than 20 dB in the low frequency range. The convergence of the solution due to the truncation effects of the infinite modal series has also been studied carefully. This effect is more important in the receiving room, which is excited acoustically via the partition. For the source room, the pressure field is dominated by the primary source, and there are not convergence problems. On the other hand, the number of modes to reach convergence in the receiving room makes the modal method very time-consuming. Although the coupled influence on the source room is not very noticeable, a fully coupled model has been maintain in the numerical simulations, because the influence of the coupling also varies with the number of normal modes employed.

The feasibility of the diffuse field reproduction with an array of near field loudspeakers and microphones has been studied separately in the three different situations. The results obtained have also been compared with the same array of near field loudspeakers driven directly with uncorrelated references signals, without an optimisation procedure. For the aluminium partition in free field conditions and coupled to the source room, there are not significant differences in the sound reduction index when using an array of optimised or uncorrelated loudspeakers. Although differences appears in the reproduction of the excitation and the response, the ratio between the incident power on the panel by the radiated power to free space does not show important discrepancies. In contrast, when the comparison is made with the classical formulation using a number of far field loudspeakers, the improvement in the sound reduction index is clearly seen in the low frequency range. The near field

array of loudspeakers is able to remove the modal effect of the cavity and to provide a measure of the sound reduction index only dependent on the panel characteristics.

The results for the transmission suite configuration, on the other hand, do not show any improvement with the near field array. The coupling between the source and receiving room through the partition is not strong enough for the optimisation in the first cavity to have an influence in the second cavity. So, for the practical application of this method, it would be necessary to used a receiving room very quiet and not reverberant, as in the case of an anechoic chamber, and to measure the incident power over the array of microphones situated on the panel, and the radiated power using the intensity method.

6. REFERENCES

Beranek, L. L. and Vér, I. L., 1992. **Noise and Vibration Control Engineering. Principles and Applications**. John Wiley & Sons, New York.

Baumann, W. T., Saunders, W. R. and Robertshaw, H. R., 1991. "*Active suppression of acoustic radiation from impulsively excited structures*". Journal of the Acoustical Society of America **90** (), 3202-3208.

Bobrovnitskii, Y. I. and Tomilina, T. M., 1995. . "*General properties and fundamental errors of the method of equivalent sources*". Acoustical Physics, **41** (5), 649-660.

Bullmore, A. J., Nelson, P. A., Curtis, A. R. D. and Elliott, S. J., 1987. "*The active minimisation of harmonic enclosed sound fields, part II: A computer simulation*", Journal of Sound and Vibration **117** (1), 15-33.

Cazzolato, B., 1999, **Sensing Systems for Active Control of Sound Transmission into Cavities**. Ph.D. Dissertation, The University of Adelaide.

Croker, M. J., Raju, P. Q. and Forssen, B., 1981. "*Measurements of transmission loss of panels by the direct determination of transmitted acoustic intensity*". Noise Control Engineering 16 (1), 6-11.

Cunefare, K. A., 1991. "*The minimum multimodal radiation efficiency of baffled finite beams*". Journal of the Acoustical Society of America **90** (), 2521-2529.

Dowell, E., Gorman III, G. and Smith, D., 1977. "*Acoustoelasticity: General theory, acoustic natural modes and forced response to sinusoidal excitation, including comparisons with experiments*", Journal of Sound and Vibration **52** (4), 519-542.

Elliott, S. J. and Johnson, M. E., 1993. "*Radiation modes and the active control of sound power*". Journal of the Acoustical Society of America **94** (4), 2194-2204.

Elliott, S.J., Gardonio, P. and Maury, C., 2001. "*A feasibility study for the laboratory simulation of turbulent boundary layer pressure fields*", Proceedings of the 7th AIAA/CEAS Aeroacoustics Conference, AIAA 2001-2194.

Elliott, S. J., 2000. **Signal Processing for Active Control**, Academic Press, London.

Egan, M. D., 1972. **Concepts in Architectural Acoustic**, McGraw-Hill Book Co., New York.

Fahy, F., 1985. **Sound and Structural vibration: Radiation, Transmission and Response**, Academic Press, London.

Fahnline, J. B. and Koopmann, G. H., 1996. "*A lumped parameter model for the acoustic power output from a vibrating structure*". Journal of the Acoustical Society of America **102** (1), 179-192.

Fahnline, J. B. and Koopmann, G. H., 1997. "*Numerical implementation of the lumped parameter model for the acoustic power output of a vibrating structure*". Journal of the Acoustical Society of America **100** (6), 3539-3547.

Fuller, C. R., Elliott, S. J. and Nelson, P. A., 1996. **Active Control of Vibration**. Academic Press, London.

Garcia-Bonito, J., 1996, **Local Active Control in Pure Tone Diffracted Diffuse Sound Fields**. Ph.D. Thesis, The University of Southampton.

Jayachandran, V., Hirsch, S. M. and Sun, J. Q., 1998. "*On the numerical modelling of interior sound fields by the modal function expansion approach*", Journal of Sound and Vibration **210** (2), 243-254.

Jo, C. H., 2000, **Active Control of Low Frequency Sound Transmission**. MSc Thesis, The University of Southampton.

Jo, C. H. and Elliott, S. J., 1992. "*Active control of low-frequency sound transmission between rooms*". Journal of the Acoustical Society of America **92** (3), 1461-1472.

Johnson, M. E., 1996, **Active Control of Sound Transmission**. Ph. D. Thesis, The University of Southampton.

Johnson, M. E., Elliott, S. J., Baek, K. H. and Garcia-Bonito, J., 1998. "*An equivalent source technique for calculating the sound field inside an enclosure containing scattering objects*". Journal of the Acoustical Society of America **104** (3), 1221-1231.

Koopmann, G. H., Song, L. and Fahnline, J. B., 1989. "*A method for computing acoustic fields based on the principle of wave superposition*". Journal of the Acoustical Society of America **86** (6), 2433-2438.

Kropp, W. and Svensson, P. U.,1995. . "*Application of the time domain formulation of the method of equivalent sources to radiation and scattering problems*". Acustica **81**, 528-542.

Maury, C., Elliott, S.J. and Gardonio, P., 2002. "*A convergence study for the laboratory simulation of random pressure fields*", Proceedings of the Institute of Acoustics, University of Salford, United Kingdom.

Nelson, P. A., Curtis, A. R. D., Elliott, S. J. and Bullmore, A. J., 1987. "*The active minimisation of harmonic enclosed sound fields, part I: Theory*", Journal of Sound and Vibration **117** (1), 1-13.

Nelson, P. A. and Elliott, S. J., 1992. **Active Control of Sound**. Academic Press, London.

Nilsson, A.C., 1972. "*Reduction index and boundary conditions for a wall between two rectangular rooms. Part I: theoretical results*". Acustica 26, 1-18.

Ochmann, M., 1995. "*The source simulation technique for acoustic radiation problems*". Acustica **81**, 512-527.

Pan, J. and Bies, D., 1990. "*The effect of fluid-structural coupling on sound waves in an enclosure-Theoretical part*", Journal of the Acoustical Society of America **87** (2), 691-707.

Pan, J., 1992. "*The force response of an acoustic-structural coupled system*", Journal of the Acoustical Society of America **91**(2), 949-956.

Panneton, R. and Atalla, N., 1996. "*Numerical prediction of sound transmission through finite multiplayer systems with poroelastic materials*", Journal of the Acoustical Society of America **100**(1), 346-354.

Pierce, A. D., 1981. **Acoustics, an Introduction to its Physical Principles and Applications**. Mc-Graw Hill, New York.

Pope, L., 1971. "*On the transmission of sound through finite closed shells: Statistical energy analysis, modal coupling and non-resonant transmission*", Journal of the Acoustical Society of America **50** (3), 1004-1018.

Quirt, J. D., 1982. "*Sound transmission through windows I. Single and double glazing*", Journal of the Acoustical Society of America **72** (3), 834-844.

Sgard, F. C., Atalla, N. and Nicolas, J., 2000. "*A numerical model for the low frequency diffuse field sound transmission loss of double-wall sound barriers with elastic porous linings*", Journal of the Acoustical Society of America **108** (6), 2865-2872.

Snyder, S. and Hansen, C., 1994. "*The design of systems to actively control periodic sound transmission into enclosed spaces, Part 1: Analytical models*", Journal of Sound and Vibration **170** (4), 433-449.

Song, L., Koopmann, G. H. and Fahnline, J. B., 1991. "*Numerical errors associated with the method of superposition for computing acoustic fields*". Journal of the Acoustical Society of America **89** (6), 2625-2633.

Utley, W.A., 1968. "*Single leaf transmission loss at low frequencies*", Journal of Sound and Vibration **8** (2), 257-261.

Vitiello, P., Nelson, P. A. and Petyt, M., 1989. "Numerical studies of the active control of sound transmission through double partitions". ISVR Technical Report No. 183.

APENDIX. THE USE OF THE EQUIVALENT SOURCE METHOD AS AN ALTERNATIVE TO CALCULATE THE SOUND FIELD INSIDE AN ENCLOSURE WITH A FLEXIBLE PANEL IN ONE WALL

The equivalent source technique was originally proposed as a simplification to the boundary elements to compute the exterior acoustic fields of arbitrarily shaped radiators (Koopmann et al., 1989). In this method, the acoustic field of a complex radiator is reconstructed as a superposition of fields generated by an array of sources inside the radiator. A set of nodal points over the surface is identified, and the magnitude and phase for the strength of each source is determined to give the correct pressure and velocity and each node point.

The mathematical formulation of the method is based on the Kirchhoff-Helmholtz integral, that states that the sound pressure field created inside a volume by sources outside can be determined totally by the normal particle velocity and pressure at the boundary. The time domain formulation has been also developed (Kropp, and Svensson, 1995). Koopmann *et* al. have shown mathematically that the Kirchhoff-Helmholtz integral is equivalent to the superposition integral, that uses the free-field Green's function to directly calculate the acoustic field due to the internal and equivalent sources, as:

$$p(\mathbf{x})=\mathrm{j}kc\rho\left[\int_{V_{\mathrm{int}}} q(\mathbf{x}_0)G(|\mathbf{x}-\mathbf{x}_0|)\mathrm{d}V_{\mathrm{in}}+\int_{V_{\mathrm{ext}}} q(\mathbf{x}_e)G(|\mathbf{x}-\mathbf{x}_e|)\mathrm{d}V_{\mathrm{ext}}\right], \tag{1}$$

where k is the acoustic wavenumber, c is the speed of sound and ρ is the density of the fluid. The internal sources are positioned at $\mathbf{x}_0$ and the equivalent sources are positions at $\mathbf{x}_e$.

In matricial formulation, the pressure field at a finite number of evaluation positions on the boundary, at a fixed frequency, can be expressed as:

$$\mathbf{p}=\mathbf{p}_{\mathrm{int}}+\mathbf{p}_{\mathrm{ext}}=\mathbf{p}_{\mathrm{int}}+\mathbf{Z}_e\mathbf{q}_e, \tag{2}$$

where the pressure at the boundary due to the sources inside the volume is given by $\mathbf{p}_{\mathrm{int}}$, and the pressure at the boundary due to the external sources is given by $\mathbf{p}_{ext}$. $\mathbf{Z}_e$ is the matrix of complex transfer impedances between the evaluation positions and the equivalent sources, and $\mathbf{q}_e$ is the vector of source strengths of the equivalent sources. The elements of the impedance matrix $\mathbf{Z}_e$ are calculated using the free-field Green's function by

$$Z_{e_{mn}}=\mathrm{j}kc\rho G\left(\left|\mathbf{x}_{s_m}-\mathbf{x}_{e_n}\right|\right), \tag{3}$$

where $\mathbf{x}_{s_m}$ is the position of the mth evaluation position and $\mathbf{x}_{e_n}$ is the position of the nth equivalent source.

The normal particle velocity can be similarly described by

$$\mathbf{u} = \mathbf{u}_{\text{int}} + \mathbf{u}_{ext} = \mathbf{u}_{\text{int}} + \mathbf{T}_e \mathbf{q}_e , \tag{4}$$

where $\mathbf{T}_e$ is the matrix that relates the particle normal velocities to the external source strengths, whose elements are calculated as

$$T_{e_{mn}} = \frac{-\partial G\left(\left|\mathbf{x}_{s_m} - \mathbf{x}_{e_n}\right|\right)}{\partial \mathbf{n}_m}, \tag{5}$$

where $\mathbf{n}_m$ is the normal to the surface at the mth evaluation position.

If the pressure and the normal particle velocity at the nodal points are related by an admittance matrix $\mathbf{Y}_b$ which characterised the behaviour of the boundary, then

$$\mathbf{u} = \mathbf{Y}_b \mathbf{p} , \tag{6}$$

where $\mathbf{Y}_b$ is a matrix of *in vacuo* self and transfer admittance for every point on the boundary assuming that the external sound field has no effect. From Eqs. (2), (3) and (4) we obtain

$$\mathbf{u}_{\text{int}} + \mathbf{T}_e \mathbf{q}_e = \mathbf{Y}_b \left[\mathbf{p}_{\text{int}} + \mathbf{Z}_e \mathbf{q}_e\right]. \tag{7}$$

If the number of equivalent sources is the same than the evaluation positions on the boundary, the optimal source strengths to produce the desired boundary conditions are given by

$$\mathbf{q}_e = -\left[\mathbf{T}_e - \mathbf{Y}_b \mathbf{Z}_e\right]^{-1} \left[\mathbf{u}_{\text{int}} - \mathbf{Y}_b \mathbf{p}_{\text{int}}\right]. \tag{8}$$

To avoid large variation in admittance between the evaluation positions, it is advised to use a larger number of evaluation points than equivalent sources. In this case, the optimal source strengths is expressed as

$$\mathbf{q}_e = -\left[\left(\mathbf{T}_e - \mathbf{Y}_b \mathbf{Z}_e\right)^{\mathrm{H}} \left(\mathbf{T}_e - \mathbf{Y}_b \mathbf{Z}_e\right)\right]^{-1} \cdot \left(\mathbf{T}_e - \mathbf{Y}_b \mathbf{Z}_e\right)^{\mathrm{H}} \left[\mathbf{u}_{\text{int}} - \mathbf{Y}_b \mathbf{p}_{\text{int}}\right]. \tag{8}$$

The equivalent source method for a rectangular room with a flexible panel

In this section, the coupling problem between a room and a vibrating surrounding structure has been addressed. As it has been observed previously, with the modal analysis of the coupled behaviour of the system the velocity predicted at the partition does not converge towards the exact value. The pressure field is accurate in the interior of the cavity but can differ substantially in the vicinity of the vibrating surface. To overcome this problem, the equivalent source technique has been applied.

Although this method has been focused mainly in the radiation from structures of arbitrary shapes (Ochmann, 1995; Fahnline and Kooopmann, 1996; 1997), it has also been used previously by Johnson *et* al. (1998) to study the behaviour of an enclosure with internal objects inside which scatter the sound. As the equivalent source method calculates both the direct field from the primary source and

the reverberant field form the boundary using the free-field Green's function, it can accurately model the behaviour close to a source without convergence problems.

A schematic representation of the physical arrangement used for the numerical simulations is shown in Figure A1. The geometrical properties of the system, Table A1, have been chosen in agreement with those of Johnson et al. (1998), for a real enclosure in the ISVR. A monopole source was situated in one corner of the room, and one microphone at the opposite corner, close to the flexible aluminium panel.

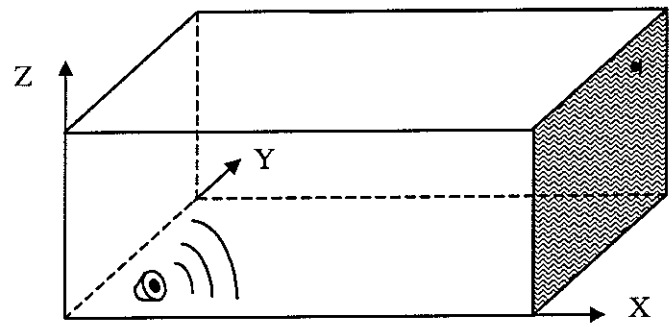

Figure A1. Physical arrangement of coupled system

Table A1. Geometrical properties used for the numerical simulation

Source room	*Dimensions*	6.06 x 2.12 x 2.12 m
	Absorption coefficient	0.036
	Source position	0.26 x 0.26 x 0.26 m
	Microphone position	5.96 x 2.02 x 2.01 m
Panel	*Dimensions*	2.12 x 2.12 m
	Thickness	0.032 m
	Damping	0.01

For the positioning of the equivalent sources, the reflection from the enclosure walls can be modelled using a number of equivalent sources placed outside the enclosure. Only the first internal source images layer has been situated close to the enclosure, along with a sphere of far-field sources, to achieve good matching at the boundary. A total of 26 image sources and 196 far-field sources have been employed in a three dimensional simulation. For the boundary, 546 evaluation positions have been employed, distributed over a grid of 10 nodal point along the x-axis, 5 along the y-axis and 5 along the z-axis.

Using this configuration, the equivalent source method has been used to calculate the sound pressure field between the source and the microphone in the rectangular enclosure when all the walls are

supposed to be rigid. The frequency response is represented in Figure A2, using a modal method and the equivalent source technique. As it can be seen the matching is very good over the whole frequency range.

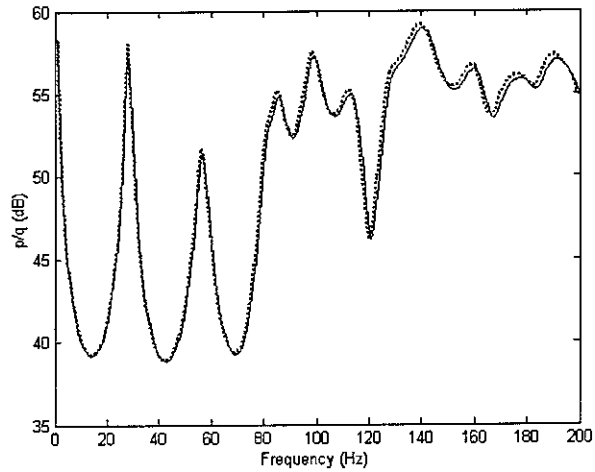

Figure A2. Frequency response of the rectangular enclosure between the source and the microphone using a modal method (solid line) and the equivalent source method (dotted line)

The same distribution of secondary sources and evaluation boundary positions has been used to calculate the sound pressure field in the cavity with the flexible panel, as shown in Figure A1. The panel has been taken as simply supported, and the mobility matrix has been calculated using standard modal theory. Three different thicknesses have been employed for the aluminium panel. The frequency response between the primary source and the microphone with the equivalent source technique is again compared with the modal method.

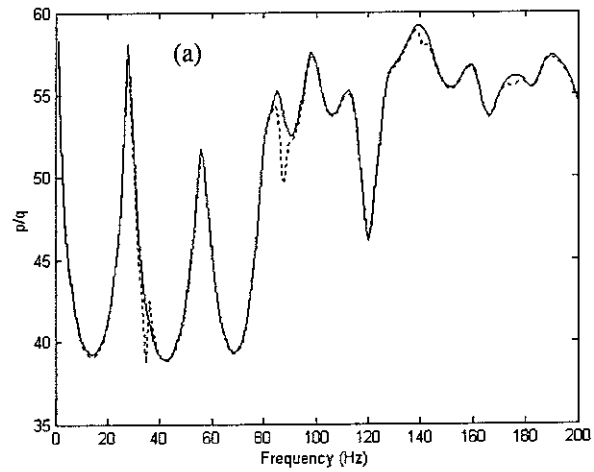

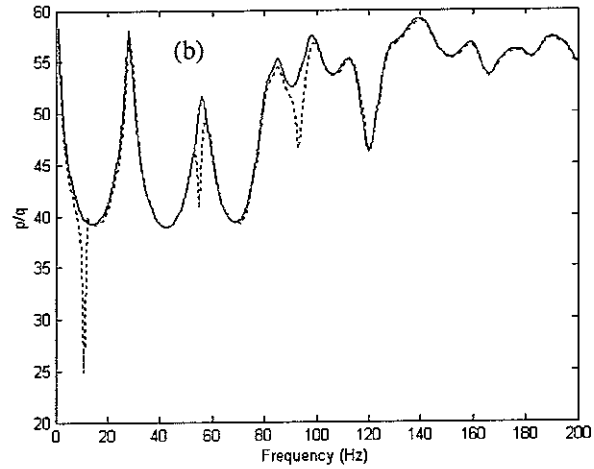

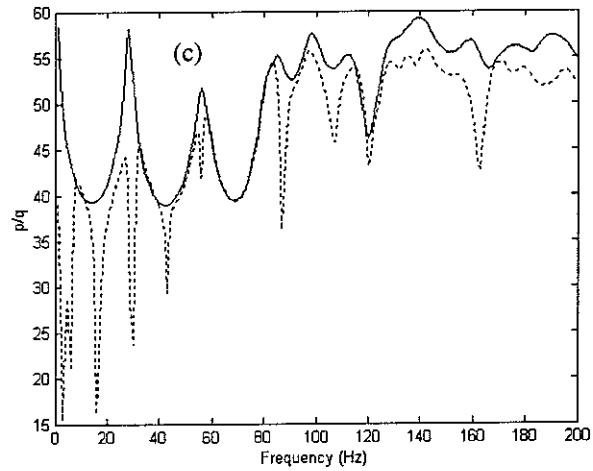

Figure A3. Frequency response of the rectangular enclosure between the source and the microphone using a modal method (solid line) and the equivalent source method (dotted line) when there is a 0.032 m (a), 0.01 m (b) and 0.0032 m (c) thick panel in one wall

As it can be seen, as the panel thickness becomes smaller, the frequency response at the normal panel frequencies becomes less accurate. For a better understanding of the results presented, an error criterion for the optimisation of the equivalent source strengths has been analysed. In this case, it has been taken as the squared normal velocity at the evaluation positions normalised by the squared normal velocity due to the internal source (Johnson et al., 1998), as

$$E = \frac{(\mathbf{u} - \mathbf{Y}_b\mathbf{p})^{\mathrm{H}}(\mathbf{u} - \mathbf{Y}_b\mathbf{p})}{(\mathbf{u}_{\mathrm{int}} - \mathbf{Y}_b\mathbf{p}_{\mathrm{int}})^{\mathrm{H}}(\mathbf{u}_{\mathrm{int}} - \mathbf{Y}_b\mathbf{p}_{\mathrm{int}})}. \tag{9}$$

Two approximations have been used in the equivalent source technique: the finite number of boundary evaluation positions and the finite number of equivalent sources for the determination of the source strengths. To analyse the convergence of the normal velocity not only at the evaluation positions, but also in a coarser grid with an extra number of monitoring point. For the configuration studied here, the monitoring positions are three times closer than the evaluation points. The results for the error in the case of the rigid walls, and a panel with different thicknesses are presented in Figures A4, A5 and A6 respectively.

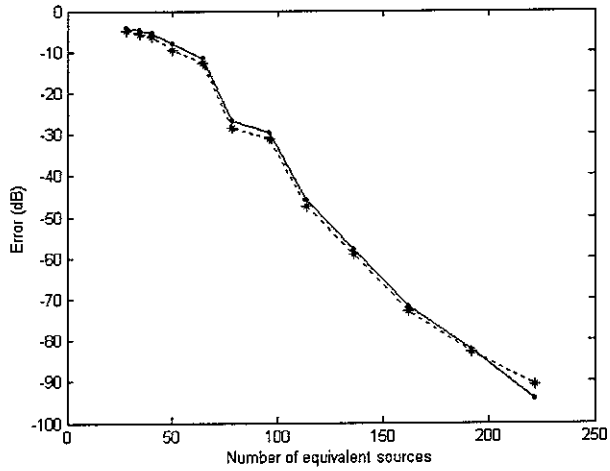

Figure 4. The error at the 2250 monitoring positions on the surface of the rigid enclosure using varying numbers of equivalent sources (dotted) and the error at the 546 evaluation positions (solid) at 88 Hz

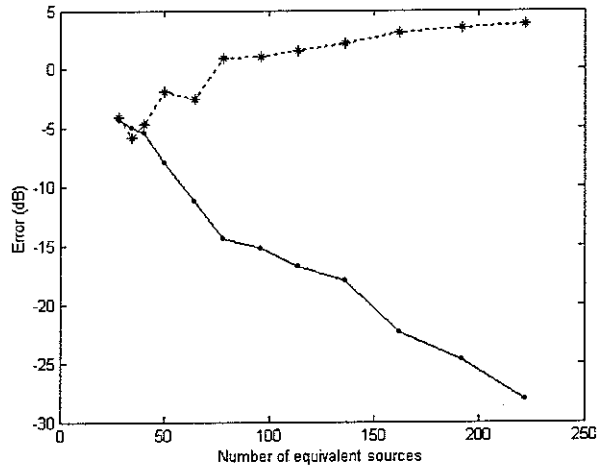

Figure 5. The error at the 2250 monitoring positions on the surface of the enclosure with a 0.032 m panel using varying numbers of equivalent sources (dotted) and the error at the 546 evaluation positions (solid) at 87 Hz

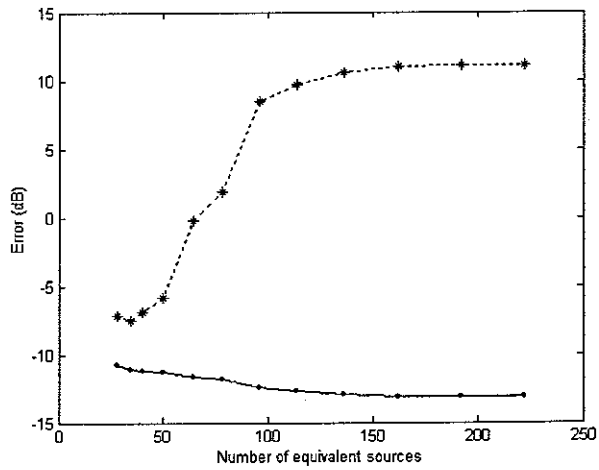

Figure 6. The error at the 2250 monitoring positions on the surface of the enclosure with a 0.01 m panel using varying numbers of equivalent sources (dotted) and the error at the 546 evaluation positions (solid) at 11 Hz

As it can be observed, with this particular configuration the problem is perfectly well conditioned for the rigid cavity. Both the errors in the evaluation and monitoring positions decrease with an increasing number of equivalent sources, and fall below 80 dB. The situation changes radically with the introduction of a vibrating surface in one wall. Although he error at the evaluation boundary position still decreases below 30 dB, there is a clear increase in the monitoring positions that it is not reduced when using a bigger number of equivalent sources. The situation is even worse for the 0.01 m thick panel.

The velocity/volume velocity transfer functions for a 0.032 m and 0.0032 m thick panel have been compared in Figure A7. As it can be appreciated, the response of the thick panel is small, with differences greater then 40 dB with respect to the thin panel. It could be that this particular configuration for evaluation positions and equivalent sources is able to provide very good results in the case of hard-walled boundary conditions, or when the boundary does not deviate too much from the rigid case, but it is not able to give a proper answer when variation to this condition start to appear.

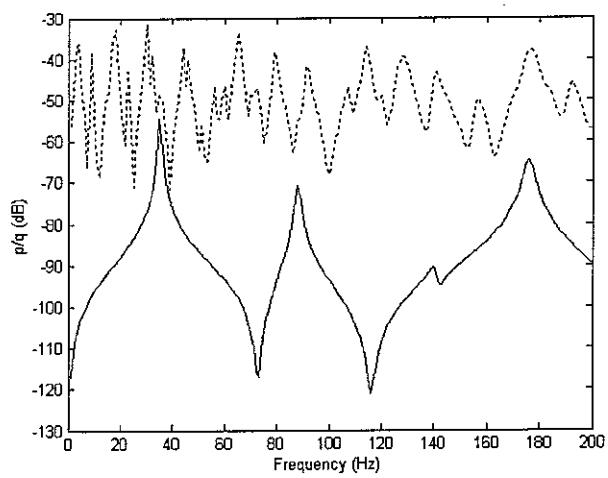

Figure A7. Velocity/volume velocity transfer function for 0.032 m thick panel (solid) and for a 0.0032 m thick panel (dotted)

This hypothesis can be also validated considered the case when one face of the enclosure is considered to be a pressure release boundary with all the other faces rigid. The frequency response and the error in the boundary and monitoring positions are represented in Figures A8 and A9, respectively. As it can be appreciated, although the error is not the same for the evaluation and monitoring positions, the values are so low that the reproduction can be considered as very reasonable.

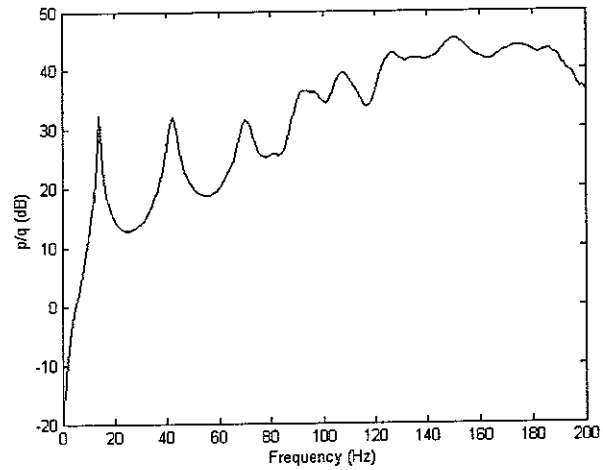

Figure A8. Frequency response of the rectangular enclosure between the source and the microphone using with one pressure release boundary

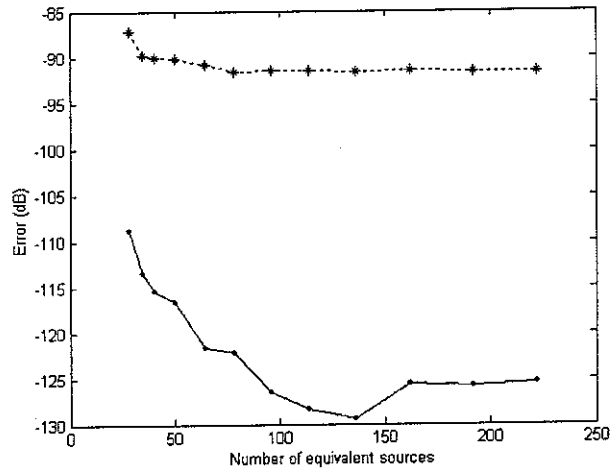

Figure A9. The error at the 2250 monitoring positions on the surface of the enclosure with a pressure release condition using a varying numbers of equivalent sources (dotted) and the error at the 546 evaluation positions (solid) at 11 Hz

So it seems that this configuration is not able to handle the problem when the boundary conditions deviate from rigid walls, and it is a convergence issue in the monitoring points. Kropp and Svensson have also found a similar result when analysing a rectangular box for which only the front was radiated. They stated that the method provides good results if the velocity distribution does not contain sudden changes in amplitude or phase. Otherwise, a check of the velocity distribution shows deviations from the prescribed conditions.

In dealing with the thin panel, although the number of evaluation positions and equivalent sources has been increased up to one point where the computational time was exorbitant, not significant improvement in the error convergence was appreciated. To study a simpler and more straightforward case, an equivalent two-dimensional configuration has been analysed, as shown in Figure A10 and Table A2. An identical simulation has been performed in the two-dimensional cavity with a flexible

bar in one side. The frequency response for a 3 mm thick bar is presented in Figure A11, and compared with the results for a rigid cavity.

Figure A10. Physical arrangement of coupled system in a two-dimensional configuration

Table A2. Geometrical properties used for the numerical simulation in a two-dimensional configuration

Source room	*Dimensions*	6.06 x 2.12 m
	Absorption coefficient	0.036
	Source position	0.26 x 0.26 m
	Microphone position	5.96 x 2.02 m
Bar	*Dimensions*	2.12 m
	Thickness	0.032 m
	Damping	0.01

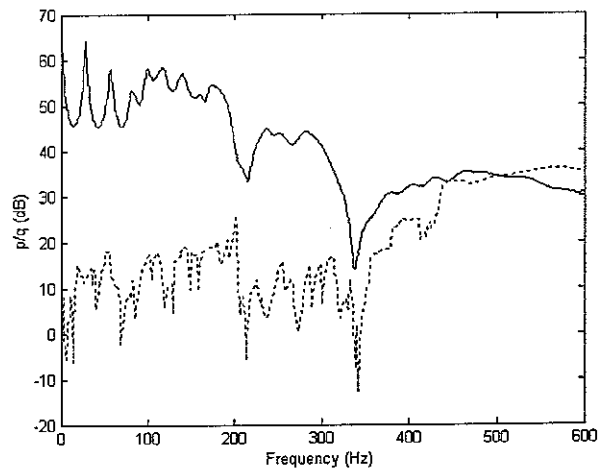

Figure A11. Sound pressure level in a two dimensional cavity with a 0.003 m thick flexible bar: rigid cavity (solid) and equivalent sources method (dotted)

The results in the two-dimensional simulation show the same trend than before. For a thin panel which varies considerably from hard-wall conditions, the equivalent source method becomes inaccurate. To study the convergence for the 3 mm panel, the number of evaluation positions and equivalent sources has been increased by a factor of 10 (Figure A12) with respect to the rigid case. Although an improvement is achieved, the method has not yet converged, and in a three dimensional simulation it

would not be possible to do the same, because it would be necessary to use 4000 equivalent sources and 6000 evaluation positions.

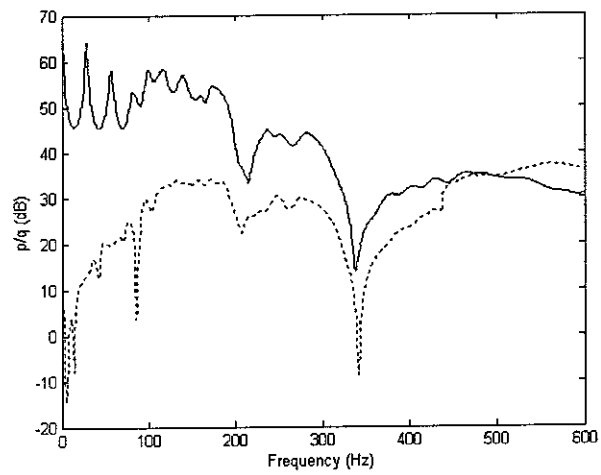

Figure A12. Sound pressure level in a two dimensional cavity with a 0.003 m thick flexible bar using 400 equivalent sources and 580 evaluation positions

Other configurations slightly different have been tested for the three dimensional case. When running the numerical simulations it was observed the response of the image sources close to the enclosure remains stable with the thickness plate, whereas it was the response of the far-field sphere sources that caused the inaccuracy. Based on this observation, different layer of images sources were positioned around the enclosure to account for the far-field effects instead of the sphere equivalent sources with a total number of 26 sources (first layer); 124 sources (second layer), 342 (third layer) and 728 (fourth layer). No significant improvement was observed. So, it does not seem reasonable to apply this method for calculating the sound reduction index in the transmission suite, either for the near or far field.

Conclusions

The equivalent sources method has been proposed as an alternative to the BEM to calculate the radiated sound filed of structures with arbitrary shape. This technique consists in enclosing an array of sources within the radiator and computing the source strengths necessary to give the specified velocities on the surface at a certain number of evaluation points.

The BEM is an established numerical method, with commercial program packages available. Basically, the sources are located on the surface of the radiator and only monopoles and dipoles are used. No source system must be constructed explicitly, so the application of the method is easier and more automatic that the source simulation technique, but very time consuming. The equivalent source method offers the advantages of simplicity and reduced computational time but it is difficult and needs experience, because no general rule exists for the source system, and numerical instabilities can occur.

In particular, the model of the behaviour of an enclosure with mixed boundary conditions presents serious difficulties of convergence.

This method is formulated in such a way that the normal surface velocities will always be exactly reproduced at the evaluation positions but there will be always error in the monitoring positions. Also, the positions of the equivalent sources can be chosen arbitrarily in principle, but they will influence the quality of the result. Some studies in the general properties of the method and an analysis of its main errors have shown that a complicated theory stands behind the superficial simplicity and not all question of this theory have been answered (Song et al., 1991; Bobrovnitskii and Tomilina, 1995). Bobrovnitskii and Tomilina have shown that the loss of accuracy at frequencies of resonance means that the set of fields of equivalent sources is functionally incomplete, and dependent on the location of the sources and evaluation positions.